Materials Today Sustainability 25 (2024) 100636

Contents lists available at ScienceDirect

Materials Today Sustainability

journal homepage: www.journals.elsevier.com/materials-today-sustainability

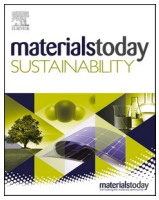

Characterization of PLA feedstock after multiple recycling processes for large-format material extrusion additive manufacturing

Alessia Romani [a,b,*], Lorenzo Perusin [a], Mattia Ciurnelli [c], Marinella Levi [a]

[a] Department of Chemistry, Materials and Chemical Engineering "Giulio Natta", Politecnico di Milano, Piazza Leonardo da Vinci 32, 20131, Milano, Italy
[b] Design Department, Politecnico di Milano, Via Durando, 20158, Milano, Italy
[c] Superforma S.r.l., Via Baldinucci 25/A, 20158, Milano, Italy

ARTICLE INFO

Keywords:
3D printing
Fused filament fabrication (FFF)
Fused granular fabrication (FGF)
Recycling
Polylactic acid (PLA)
Distributed recycling for additive manufacturing (DRAM)

ABSTRACT

Since the take-make-dispose model is leading to significant waste production and environmental impact, circular economy models have been spreading to reduce waste and resource depletion, rethinking the existing resource cycles. Plastic waste created environmental and economic concerns, requiring new recycling methods and strategies to preserve resources. This practice plays a key role in extrusion-based additive manufacturing, converting waste into recycled feedstock. Large-format additive manufacturing represents a promising way to scale up recycling strategies with granulated polymer feedstock, especially considering popular materials, i.e., PLA. However, thermomechanical degradation affects the quality of this secondary raw material, and these effects on large-format systems are scarcely studied. This work investigates the thermal, rheological, and mechanical properties of PLA feedstock for large-format additive manufacturing after multiple recycling processes, i.e., up to six. The effect of material degradation from multiple recycling processes was assessed through Gel Permeation Chromatography, Differential Scanning Calorimetry, flow stress ramp tests, tensile tests, and colorimetry. Some 3D printed parts were fabricated to assess the overall quality of the process, including pieces from potential applications. Lower effects of thermomechanical degradation were found compared to desktop-size 3D printers, mainly by cutting the reprocessing steps to produce secondary raw materials, i.e., making new filaments. Recycled granulate PLA feedstocks represent a potential alternative to virgin pellets for new applications in real-world contexts.

1. Introduction

The traditional linear model of production has been the dominant economic model for decades. However, companies are now realizing that this approach poses environmental and economic risks, particularly in terms of raw materials [1,2]. Sustainability aspects connected to production and consumption should be, therefore, considered throughout the whole lifecycle of materials and products [3]. For instance, most of the environmental impacts and production costs of new goods are strongly influenced by the early stages of the design process [4,5]. Sustainability metrics tools, such as Life Cycle Assessment (LCA), can support the design and development process, as well as new approaches to encourage the spread of new sustainable practices and economic models, e.g., distributed manufacturing [3,5,6]. The centralized take-make-dispose model has resulted in significant waste generation and environmental impact, leading companies to embrace new concepts, such as the circular economy [7,8]. Circular economy aims to reduce waste, pollution, and resource depletion by rethinking existing cycles of energy and resources by keeping them in use [9,10]. Initially based on the principles of reduce, reuse, and recycle (the 3Rs), the circular economy has evolved to include additional strategies such as reuse, remanufacture, and repurpose, i.e., through the 10Rs model [11,12]. Transitioning to a circular economy for plastics requires investments and risks, but it can reduce waste, energy consumption, and greenhouse gases (GHG) emissions, preserve virgin resources, and unlock new design and economic opportunities [13–15]. Estimates suggest that the circular economy could represent up to two-thirds of the total profit growth pool for the petrochemical-plastic industry by 2030 [16].

* Corresponding author. Department of Chemistry, Materials and Chemical Engineering "Giulio Natta", Politecnico di Milano, Piazza Leonardo da Vinci 32, 20131, Milano, Italy.
E-mail address: alessia.romani@polimi.it (A. Romani).

https://doi.org/10.1016/j.mtsust.2023.100636
Received 29 August 2023; Received in revised form 10 November 2023; Accepted 6 December 2023
Available online 10 December 2023

Plastic waste presents a significant challenge, both environmentally and economically. By 2050, the GHG emissions from the plastic sector are expected to reach ~15 % of the global annual carbon budget, increasing their impact by 15 times [17]. In addition, only around 30 % of plastic is effectively recycled, with the rest used for energy recovery or in landfills [18]. Various recycling methods exist, from mechanical processes like shredding and remelting to chemical recycling techniques [19]. Each recycling process offers unique advantages and limitations, depending on the nature and condition of the materials [20]. Although recycling may result in lower-quality materials, i.e., downcycling, it significantly curtails CO_2 emissions associated with manufacturing processes by reducing the demand for new raw materials [13,21]. Furthermore, it usually involves a systematic collection and reprocessing of materials and products at their End-of-Life [21]. Combined with specific design strategies, it allows to transform waste into high-value products or raw materials for various applications, i.e., upcycling [13,22,23].

Recycling also plays a crucial role in the field of additive manufacturing (AM) [24–27]. These technologies, commonly known as 3D printing, fabricate three-dimensional objects by adding different layers of material [28]. However, they can generate substantial waste, including failed 3D printed parts, support materials, and old prototypes [29,30]. Recycling offers a viable approach to managing possible waste, converting it into new recycled feedstock for further processing, such as filaments or pellets for Material Extrusion AM [29,31]. These AM processes, i.e., Fused Deposition Modeling (FDM, also known as Fused Filament Fabrication, FFF), involve the extrusion and selective deposition of melted or viscous materials using a nozzle, i.e., thermoplastics [32]. Desktop-size small-format 3D printers usually represent the common size of FDM/FFF apparatuses thanks to their accessibility for the end-users [33]. However, previous works demonstrated the higher energy consumption, hence environmental impacts, of FFF when considering the production of raw materials used in this technology, generally, spool filaments obtained through extrusion processes [34,35]. Moreover, fabricating parts requiring long building times also increases the energy consumption of FFF, and medium or big parts cannot be produced with small-format 3D printing systems, limiting their range of potential applications [35,36]. To this extent, Large-Format AM (LFAM, or Large-Scale AM, LSAM) allows the production of parts with significantly large dimensions, with a building volume equal to or higher than 1 m^3 [37]. Unlike desktop-size 3D printers, extrusion-based LFAM often utilizes granulate or pellet feedstock for the deposition of larger quantities of polymers or polymer-based composites, i.e., Fused Granular Fabrication (FGF) processes [37,38]. This approach offers several advantages, including higher 3D printing speeds, reduced material degradation, and a wider range of material options [36]. However, LFAM still has some drawbacks in terms of higher costs and lower accessibility, as well as technical challenges. For instance, the kinematic systems and dimensions of LFAM printers pose challenges for moving the extruder and achieving high-resolution prints, especially for bigger objects at high feed rates [39]. Thermal issues are also crucial in LFAM since maintaining an optimal deposition temperature throughout the printing process is vital to ensure good adhesion between layers and shape retention [40]. Preheating systems and effective cooling strategies are employed to manage the temperature while 3D printing larger parts [41,42]. Finally, optimizing the extrusion control during the building process and the design and manufacturing strategies strongly impact the final part, the overall 3D printing quality, and finishing [39]. Managing these constraints is essential to successfully implement LFAM in real-world contexts, making it a viable option for a wide range of industrial applications.

Recently, the use of recycled feedstock for extrusion-based AM has been progressively established for new products and applications, including bio-based materials and biomass [29,30,43–45]. To this end, Distributed Recycling for Additive Manufacturing (DRAM) contributes to spreading this approach to 3D printing [30]. The DRAM model enables prosumers to utilize both AM and traditional plastic waste to create valuable 3D printing feedstocks, as well as new consumer goods [46]. This approach fosters accessible 3D printing systems and strategies to produce locally consumed products with potential benefits from the environmental, economic, and social perspectives [47–50]. Although small-format FFF 3D printers have been used within DRAM contexts, LFAM FGF systems represent a more promising option to locally recycle plastic waste thanks to the direct use of granulate feedstock, which eliminates the reprocessing steps for filaments as secondary raw materials [49,51].

Understanding how polymers degrade and how this affects their properties is crucial for developing recycling processes for FDM/FFF and FGF at small and large scales. Polymer degradation can be due to different mechanisms [52]. Among those, thermal degradation occurs when polymers are exposed to heat, promoting chain movement and leading to degradation and decomposition. This process reduces their molecular weight, affecting mechanical, thermal, and rheological properties [53]. During Material Extrusion AM processes like FDM/FFF, polymers are exposed to thermal and oxygen effects and shear stresses. Combining these factors contributes to chain scission phenomena known as thermomechanical degradation [54]. This type of degradation is prevalent during the melting processes of polymers, particularly in materials with high melt viscosity or under high extrusion or processing speeds [55].

Polylactic Acid (PLA) is a popular material for additive manufacturing due to its good mechanical properties and ease of processing [56,57]. It is available in filament or pellet form, suitable for desktop 3D printers and larger machines. PLA can be printed without a heated bed, although its use can prevent issues like detachment or shrinking [58]. Post-processing PLA parts is straightforward, with easy removal of supports and imperfections. However, PLA, being thermodynamically unstable, is susceptible to thermomechanical degradation during processing, including recycling [59,60]. High temperatures lead to random main-chain scission reactions, resulting in rapid degradation of molecular weight and subsequent changes in the properties of 3D printed objects [54,61]. Some studies have investigated the impact of recycling on the mechanical, thermal, and rheological properties of PLA used for FDM/FFF [62–66]. Nevertheless, their focus is primarily on materials processed with desktop-size small-scale 3D printers. There is a scarcity of literature evaluating the effects of recycling on the properties of PLA printed with extrusion-based LFAM technologies, especially FGF systems, despite its potential as a scaling-up strategy in DRAM contexts. Moreover, scraps and waste from the 3D printing process itself represent a potential source of secondary raw materials for local manufacturing communities, which have recently started to close the loop through new recycling initiatives [67,68].

This work aims to study the thermal, rheological, and mechanical behavior of 3D printed PLA after multiple recycling and 3D printing processes on large-format FGF AM systems, simulating the reprocessing of scraps and waste from the 3D printing sector. It differs from previous studies as it focuses on the characterization of recycled PLA after multiple cycles, up to six, processed by an LFAM FGF 3D printer, representing a step forward from using FFF filament-based small-format systems. In detail, it compares the characterization of virgin PLA pellets and recycled PLA feedstock after multiple recycling processes, i.e., until six extrusion and recycling cycles. The effect of the processing cycles on material degradation and the variation of molecular weight was assessed through GPC analysis (Subsection 3.1). The thermal characterization of the different PLA feedstock was then performed by means of DSC tests (Subsection 3.2). A flow stress ramp test was then used to understand the rheological behavior of the material, simulating the processing conditions in the extruder chamber (Subsection 3.3). Tensile specimens were 3D printed and tested to determine the mechanical properties of the feedstock batches (Subsection 3.4). The overall 3D printing quality was assessed thanks to textured samples, also used for the colorimetry analysis. Finally, some demo applications were selected as case studies to demonstrate the use of recycled PLA feedstock after several

processing cycles, i.e., by printing cut-offs and complex geometries (Subsection 3.5). Although the influence of thermomechanical degradation and chain scission on the properties, 3D printing granulate or pellet feedstock helps limit the degradation effect by cutting the required steps to obtain secondary raw material, i.e., making filaments. Recycled PLA feedstock is a promising alternative to virgin pellets until five extrusion and recycling processes for some applications, fostering material-driven approaches to design new products with similar PLA feedstock.

2. Materials and methods

2.1. Materials

Virgin PLA feedstock was used as the starting raw material for the FGF 3D printer. PLA Ingeo 2003D was produced by NatureWorks LCC (Minneapolis, MN, US) and supplied by FiloAlfa (Torino, Italy) in the form of pellets. It was used as received as feedstock for the large-format FGF 3D printer. The recycled feedstock after one to five extrusion and recycling processes was obtained through mechanical recycling from the same 3D printed virgin PLA feedstock to allow comparisons between the different recycling processes. This choice also simulates using 3D printed PLA waste as secondary raw material for multiple recycling and FGF processes.

2.2. Experimental methods

Different characterization tests were performed on the virgin and recycled PLA feedstock, either after multiple 3D printing or shredding processes. The workflow followed during the experimental work is resumed in the flow chart of Fig. 1. Virgin PLA pellet (B0) represents the starting point. The number of extrusion processes is visible on the top, corresponding to the number of 3D printing cycles performed on the recycled feedstock. Similarly, the number of recycling processes through shredding is specified at the bottom. 3D printed samples resulted after each extrusion cycle, whereas shredded feedstock after each recycling cycle of the 3D printed part. For the sake of simplicity, each batch of samples was renamed according to the following criteria.

- B0 indicates the virgin pellet, where 0 corresponds to the number of extrusion and recycling processes. Gel Permeation Chromatography (GPC), Differential Scanning Calorimetry (DSC), and rheological tests were performed on this virgin feedstock batch.
- BX indicates the 3D printed samples after each cycle, where X corresponds to the number of extrusion processes undergone for the material. In this case, the number of recycling processes is X-1. For instance, “B2” is a batch of 3D printed samples that underwent two 3D printing extrusion cycles and one recycling cycle. GPC, DSC, tensile tests, and colorimetry were performed on these 3D printed batches.
- BYM indicates the shredded feedstock after each cycle, where Y corresponds to the number of recycling processes undergone for the material. In this case, the number of recycling processes is equal to Y. For example, “B2M” is a batch of recycled feedstock that underwent two 3D printing extrusion cycles and two recycling cycles. Rheology was performed on these shredded feedstock batches.

2.3. Mechanical recycling of PLA

3D printed PLA feedstock was recycled through mechanical recycling processes on samples processed with the LFAM system used in this work (Subsection 2.8). The material was shredded using a Rapid RG Slow-speed granulator model RG3 (Rapid Granulator AB, Bredaryd, Sweden) with a maximum grinding capacity of 20 kg/h. Big 3D printed parts were previously cut in smaller sections of ~100 mm to facilitate the shredding process, performed at a rotational speed of 60–90 rpm. The material underwent four shredding cycles to increase the dimensional homogeneity of the recycled feedstock particles. The material was then manually sieved with a mesh size of 4 mm to obtain recycled PLA feedstock for the tests. The granulometry distribution of the shredded feedstock after four shredding cycles was measured to check the homogeneity of the granulates, which strongly influences the extrudate processability with a screw pellet extruder [69]. The measurements were performed by sieving 1 kg of shredded feedstock with five different mesh sizes, i.e., 4, 3, 2, 1, and 0.5 mm, weighting the sifting leftovers of each step and sieving the sifted portion with the next finer mesh until reaching the 0.5 mm mesh size. The different values were then used to calculate the weight percentage of each dimension range and the

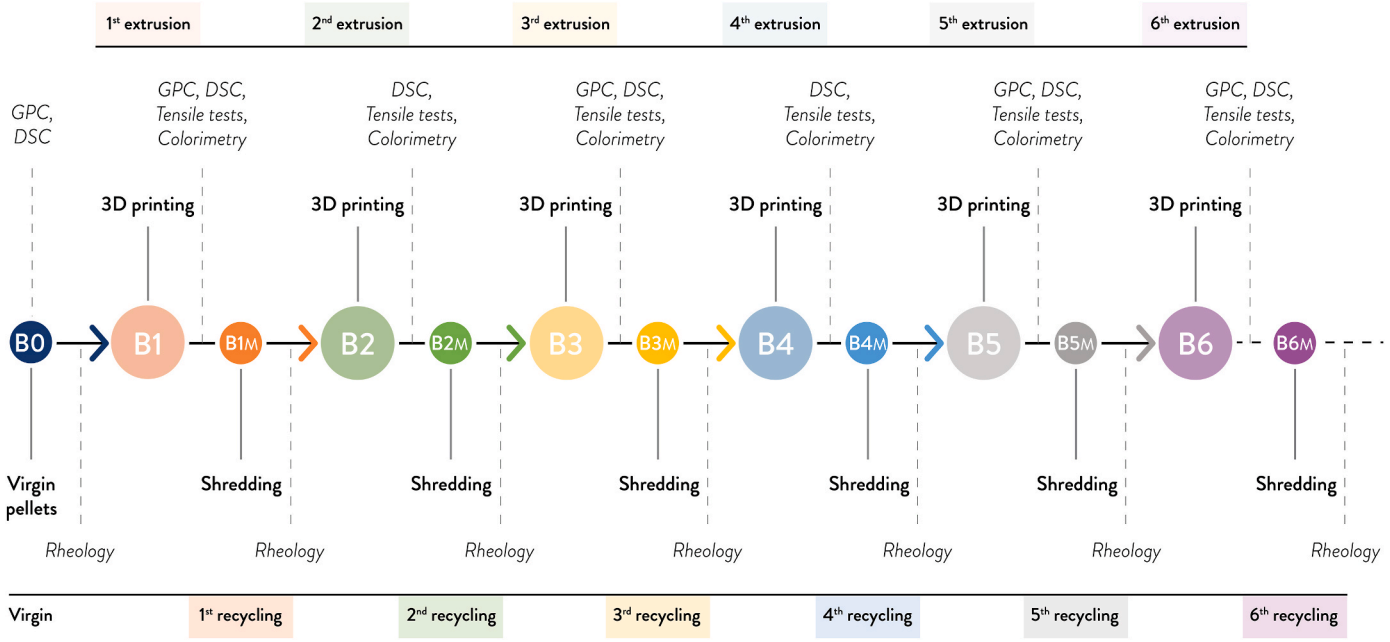

Fig. 1. Flow chart of the experimentation conducted in this work with the different 3D printing (extrusion) and shredding (recycling) steps, the test performed for each step, and the nomenclature of each sample batch.

weighted mean values of the particle size, obtaining comparable results for each batch of shredded feedstock. The recycled feedstocks, after four shredding cycles, are mainly composed of particles ranging between 2 and 4 mm (~40 % wt., between 2 and 3 mm and ~34 % wt. between 3 and 4 mm) with a low percentage of particles below 2 mm (~16 % wt. between 1 and 2 mm, ~5 % wt. between 0.5 and 1 mm, and >1 % wt. smaller than 0.5 mm, respectively) and ~4 % wt. of granulates bigger than 4 mm. The average size of the feedstock particles is ~2.5 mm, which can be easily processed with the 3D printer used in this work.

The result after the mechanical recycling is visible in Fig. 2, with the virgin pellet as a benchmark. Five different recycled feedstock materials were obtained, i.e., from B1M to B5M, corresponding to the different extrusion and recycling processes explained in Subsection 2.2 and Fig. 1.

2.4. GPC and molecular weight analysis

GPC tests were done to determine the number average molecular weight (M_n), weight average molecular weight (M_w), and polydispersity index (PDI) of PLA feedstock after the different 3D printing and recycling processes. Three batches of samples were tested with a Waters 1515 isocratic high-performance liquid chromatography (HPLC) system (Waters Corporation, Milford, MA, US): B1 as 3D printed virgin material, B3 and B5 as recycled feedstock after 3 and 5 extrusions. The samples were dissolved in tetrahydrofuran (THF) with a magnetic stirrer. The chromatographic columns were calibrated with polystyrene (PS) standards.

2.5. DSC and thermal properties

DSC analysis was used to investigate the thermal properties of the PLA batches. Tests were performed with a Mettler-Toledo DSC/823e machine (Mettler Toledo, Columbus, OH, US) on 5–25 mg samples of virgin pellet and from the 3D printed feedstock after each cycle of extrusion, i.e., from B1 to B6. Two different thermal cycles were performed. The first one consisted of three runs (heating-cooling-heating) and was done to determine the glass transition temperature (T_g), melting temperature (T_m), and the enthalpy of fusion (ΔH_m): from 25 °C to 220 °C, from 220 °C to −50 °C, and from −50 °C to 220 °C at a scan rate of 10 °C/min. The second cycle was carried out to evaluate the degree of crystallinity of PLA (χ), as well as the enthalpy of fusion (ΔH_m) and enthalpy of crystallization (ΔH_c). It consisted of a single heating ramp from 0 °C to 220 °C at a scan rate of 5 °C/min. The degree of crystallinity was calculated according to Equation (1):

$$\chi = \frac{\Delta H_m - \Delta H_c}{\Delta H_m^0} \quad \text{Eq. 1}$$

where ΔH_m is the normalized enthalpy of fusion, ΔH_c the normalized crystallization enthalpy, and ΔH_m^0 the standard fusion enthalpy for a fully crystalline sample, corresponding to 93.1 J/g [70].

2.6. Rheological tests

Rheological measurements were conducted using a Discovery HR-2 hybrid rheometer (TA Instruments Inc, New Castle, DE, US) with a 25 mm parallel steel plate geometry and 1 mm gap. The tests were performed on the different virgin and recycled feedstock samples, which means B0, B1M, B2M, B3M, B4M, B5M, and B6M (Fig. 1).

A flow stress ramp test was performed to analyze the shear behavior of the PLA batches during the extrusion process. Tests were performed for 180 s at 185 °C to simulate the optimal hot-end temperature. The applied shear rate progressively ranged from 10^{-2} to 10^{2} s^{-1}. The experimental results were then used to calculate the zero shear viscosity (η_0). The flow behavior index (n), or power law index, was calculated to approximate the flow behavior at reference shear rates simulating 20 mm/s as typical 3D printing conditions [71]. The expected shear rate was calculated according to Equation (2):

$$\dot{\gamma}_w = \frac{\pi D N}{60 H} \quad \text{Eq. 2}$$

where $\dot{\gamma}_w$ is the expected shear rate in the internal screw channel wall, D the screw diameter in mm, N the screw speed in rps, and H the channel depth in mm [72]. The flow behavior index (n) was obtained through the power law approximation, resumed in Equation (3):

$$\eta = k\dot{\gamma}^{\,n-1} \quad \text{Eq. 3}$$

where η is the viscosity, $\dot{\gamma}$ the shear rate, k the consistency, and n the flow behavior index [71].

2.7. Tensile tests

Tensile tests were performed at a 1 mm/min speed with a Zwick Roell Z010 testing machine (ZwickRoell GmbH & Co. KG, Ulm, Germany), using a 10 kN load cell and square grips. The specimens were produced and tested following the ASTM standard D638-14 [73]. At least five Type IV geometry specimens were 3D printed for each PLA feedstock, ranging from B1 to B6 and resulting in six batches [74]. The dog-bone specimens have a nominal gauge length of 33 mm, a thickness of 4 mm, and a width of 6 mm. The samples were produced by following the parameters resumed in Table 1, using a 100 % rectilinear infill and an outline overlap to avoid intralayer voids (Fig. 3). In detail, the parameter was increased up to 50 % to facilitate the overlap between the extruded path of each deposited layer. This change helped obtain specimens with a real 100 % infill by filling the voids between the perimeters and infill paths, as visible in Fig. 3a. The same parameter was used to obtain the different batches of tensile specimens, i.e., from B1 to B6 (Fig. 3b). The main asperities from the fabrication process were manually removed through sanding to ensure a constant cross-section in the gauge length. The actual measures were then obtained by using a

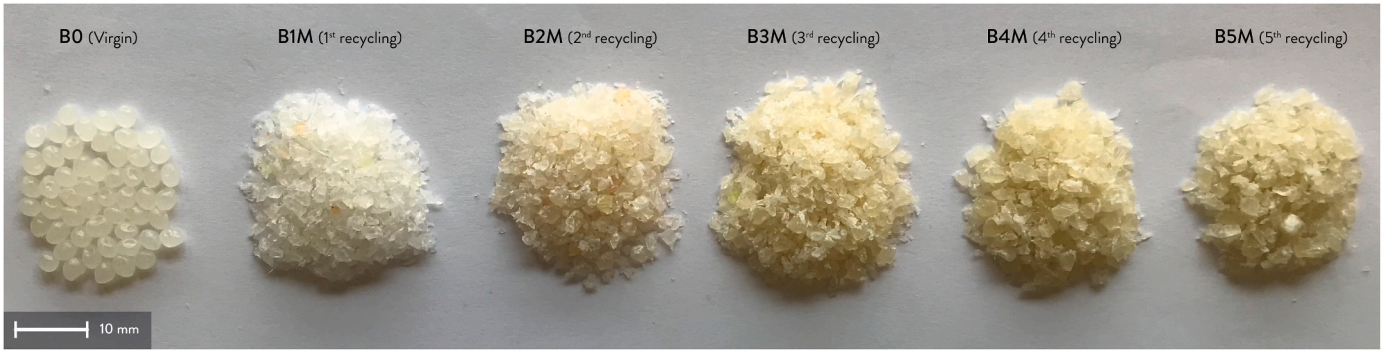

Fig. 2. PLA feedstock used in this work (from left to right): virgin pellet (B0), shredded and sieved PLA at the first (B1M), second (B2M), third (B3M), fourth (B4M), and fifth (B5M) recycling cycle.

Table 1
3D printing parameters of the tensile specimens, texture samples, and demo cut-off.

Parameter	Unit	Values		
		Tensile specimens	Texture samples	Demo cut-offs
Nozzle diameter	mm	3	3	3
Extrusion multiplier	//	0.8	0.8	0.8
Extrusion width	mm	3.8	3.8	3.8
Layer height	mm	0.7	0.7	0.5–0.7 - 1.0
Perimeters	//	1	1 (vase mode)	1
Top and Bottom layers	//	4	//	//
External fill pattern	//	rectilinear	//	//
External infill angle offsets	°	180	//	//
Outline overlap	%	50	//	//
Temperature (Extruder)	°C	185	185	180–200
Temperature (Printing bed)	°C	70	70	70
3D Printing speed	mm/s	20	8	8–12

caliper. The stress-strain curves from the experimental tests were used to calculate the mean values and standard errors of elastic modulus (E), ultimate tensile strength (σ_m), fracture strength (σ_b), elongation at maximum stress (ε_m), and elongation at break (ε_b).

2.8. Large format material extrusion additive manufacturing and 3D printed parts

A Delta Wasp 3 MT Industrial (Wasp Srl, Massa Lombarda, Italy) was selected as the large-format Material Extrusion AM system used in this work. This 3D printer is a Fused Granular Fabrication (FGF) machine based on the delta system kinematics equipped with a single screw pellet extruder, a stainless steel nozzle with a diameter of 3 mm, a heated circular bed, and a closed chamber. Its standard printing volume corresponds to a cylinder with a diameter of 1000 mm and a maximum height of 1200 mm, classifying this machine as a large-format 3D printing system [37].

Three different kinds of samples were 3D printed for the experimental work: (i) tensile specimens, (ii) texture samples, and (iii) demo cut-offs. Tensile specimens were designed according to the ASTM Standard D638-14 [73]. Texture samples helped assess the printability of the different recycled PLA feedstock and were used for the colorimetric analysis (Subsection 2.9). The samples have a nominal dimension of 88 × 88 × 90 mm, and they include an embossed and engraved diamond-textured surface with a max overhang of 30°. Their objective is to qualitatively assess the feasibility and overall quality of the process for each recycled feedstock at different layer heights. The demo cut-offs were used as a proof-of-concept and demonstrators of possible products and applications fabricated with the recycled feedstock studied in this work. Two different case studies were selected: joint cut-offs from furniture elements, such as modular chairs, and complex shapes from art replicas. The joint cut-offs have a maximum dimension of 100 × 100 × 100 mm, whereas the art replicas are cut-offs of 126 × 146 × 153 mm maximum.

The 3D printed samples were sliced with Simplify3D (Simplify3D, Cincinnati, OH, US), and the 3D printer was controlled and monitored with the open source software platform OctoPrint [75]. Table 1 shows the main 3D printing parameters of the 3D printed parts. The same parameters were used for each recycled feedstock to simulate real-world contexts, avoiding settings that could discourage their use in real applications, e.g., very low 3D printing speeds.

2.9. Colorimetric analysis

Colorimetric analysis was carried out with a Konica Minolta CM600D spectrophotometer (Konica Minolta Sensing Americas Inc, Ramsey, NJ, US) equipped with a pulsed xenon lamp with a UV cut filter. To assess the color variation after several 3D printing and recycling processes, the L*a*b* coordinates of the CIELAB color space were measured from the 3D printed texture samples of the feedstock (B1 to B6), according to the ASTM Standard D2244-21 [76]. Each specimen was measured at five different points to calculate the mean values and standard deviations after each 3D printing and recycling process. ΔL*, Δa*, Δb* (direction of the color difference), and ΔE* (discoloration) were then calculated with Equation (4):

$$\Delta E^* = \sqrt{(\Delta L^*)^2 + (\Delta a^*)^2 + (\Delta b^*)^2} \quad \text{Eq. 4}$$

where ΔL*, Δa*, and Δb* is the difference between the coordinates of

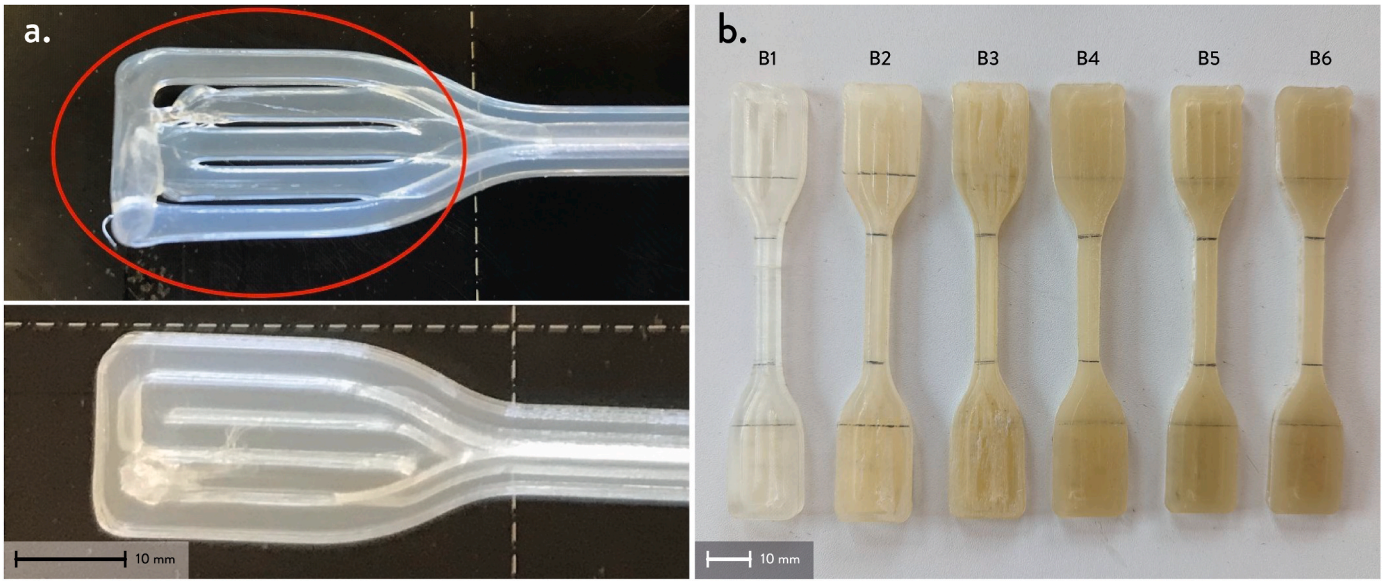

Fig. 3. Tensile specimens from PLA feedstock: (a) optimization of the process parameters to reduce the presence of voids between the extrusion paths through extrudate overlapping; and (b) comparison from the different sample batches (B1 to B6).

the samples after each 3D printing and recycling process (B2–B5) and the sample printed with virgin pellet (B1). The difference in colors is given by the signs of the direction of the color difference values: ΔL*, where positive means lighter and negative darker, Δa*, where positive means redder and negative greener, and Δb*, where positive means yellower and negative bluer.

3. Results and discussion

3.1. GPC and molecular weight analysis

The influence of the printing and recycling cycles on the different PLA feedstock is visible from the results of the GPC analyses. According to Table 2 and Fig. A1 (Appendix A), increasing the recycling steps reduces molecular weights. After the extrusion of the virgin pellets (B0 to B1), the value of the number average molecular weight (M_n) decreased from 82,939 to 70,594 g/mol, which means a reduction of −14.9 %. This reduction becomes more pronounced after three extrusions and two recycling cycles (B3), with a decrease of −27 %. After six extrusions and five recycling processes (B6), the M_n value is halved compared to the initial value, reaching 40,922 g/mol, −50.7 %.

A similar trend can be observed for the weight average molecular weight (M_w). After the first extrusion (B0 to B1), the value decreases by −16.7 %, from 116,969 to 97,385. It further decreases to −23.7 % after three extrusions and two recycling cycles (B3). After six extrusions and five recycling processes (B6), the total reduction of M_w is −47,6 %, reaching a value of 61,263 g/mol. These increasing reductions indicate the occurrence of degradation phenomena in PLA feedstock, potentially associated with chain scissions and *trans*-esterification due to the continuous thermomechanical stress that occurred during the extrusion 3D printing [19,55,62,77].

Focusing on the distribution and heterogeneity of the polymer chains, the value of polydispersity index (PDI), which means M_w/M_n, only increases by one decimal point comparing the virgin pellet (B0) and the recycled PLA feedstock after six extrusions and five recycling cycles (B6), ~1.5. This slight increase suggests a tendency toward homogeneity in the length of the polymer chains during the reprocessing cycles despite the thermomechanical degradation indicated by M_n and M_w. This fact is also visible in Fig. A1 (Appendix A), especially from the similar amplitudes of the curves from the different PLA feedstocks.

The results are consistent with previous works from literature with desktop-size 3D printers. Cruz et al. obtained comparable reductions of M_w after three extrusion and recycling cycles, ~27 %, whereas the results after the fifth cycle are similar to the values from B6, ~47 % [63]. Zhao et al. obtained lower values of M_n and M_w after two recycling cycles, ~16,000 g/mol and ~42,000 g/mol, respectively [65]. In both cases, the recycled PLA feedstock underwent a further extrusion step for each cycle to make a new filament, increasing the influence of thermomechanical degradation on chain scission. Accordingly, granulate recycled feedstock in FGF extrusion systems reduces the effect of thermomechanical degradation by cutting the extrusion steps for filaments.

3.2. DSC and thermal properties

DSC tests were performed to investigate the impact of the multiple recycling and extrusion processes on the thermal properties of PLA feedstock. As from Table 3, glass transition temperature (T_g) decreased by 1.9 °C after six extrusion cycles, from 60.5 °C to 58.6 °C. A similar behavior is observed for the melting temperature (T_m), decreasing to 2.3 °C. Therefore, no significant changes in T_g and T_m are visible, according to the curve from the second heating ramp of Fig. A2 (Appendix A). For this reason, the effect of multiple extrusion and recycling cycles on the thermal properties of PLA feedstock seems limited despite the reduction of the molecular weight that emerged from the GPC analysis. This result confirms previous work on multiple recycling of PLA feedstock after extrusion processes [64]. A significant increase in the enthalpy of fusion (ΔH_m) can be observed from batch B2 onwards. This fact could indicate an increase in the crystallinity of the material. As visible from Fig. A2 (Appendix A), exothermic peaks of cold crystallization appear within the range of 100 °C–150 °C starting from batch B2. This phenomenon occurs when sufficient energy is provided to the polymer chains, allowing them to reorganize and initiate crystallization when the temperature increases. Moreover, a double melting peak is visible in batches B5 and B6. Their presence can be linked to the presence of two crystalline structures with different T_m or the material degradation caused by the continuous melting, recrystallization, and remelting cycles during extrusions [78].

Single ramp DSC at lower temperature ramp rates was performed to evaluate the degrees of crystallinity after the different extrusion and recycling processes. Table 4 shows the values of enthalpies of cold crystallization (ΔH_c) and ΔH_m, together with the degree of crystallinity (χ). The values of ΔH_c and ΔH_m are quite similar, with a variation of ~5 J/°C in most cases. Consequently, the samples were amorphous, and most of the crystals formed during the analysis. Except for the virgin material (B0), this fact is further supported by the degree of crystallinity. After the first extrusion (B1), the value decreases and remains consistently around 4–7% for batches from B2 to B6, suggesting that the material is mainly amorphous. As reported by Gonçalves et al. [64], this result may be attributed to the distribution of molecular weights, remaining quite constant despite the reduction in M_n and M_w. As shown in Fig. A3 (Appendix A), the double melting peaks appear from batch B2, and their height gradually increases, becoming more defined. This result is consistent with the degradation increase after several extrusion and recycling cycles from the reduction of M_w [78].

3.3. Rheological tests

Rheological tests were conducted on virgin pellet material and recycled PLA feedstock (B1M-B6M) at 185 °C to replicate the conditions of the extruder chamber during the different extrusion cycles. Fig. 4 shows the curves of the flow stress ramp test, plotting the viscosity as a function of the shear rate on a log-log graph. The viscosity measured from the first Newtonian plateau progressively decreases when increasing the number of extrusion cycles. Similarly, the shear-thinning region starts at higher shear rates. According to Table 5, the zero shear viscosity (η0) decreases after each extrusion and recycling cycle. After the first cycle (from B0 to B1M), the viscosity decreases by 22.7 %

Table 2
Number average molecular weight, weight average molecular weight, and polydispersity index of 3D printed batches: virgin pellet (B0) and recycled feedstocks after one (B1), three (B3), five (B5), and six (B6) extrusion cycles.

Batch	M_n (*g/mol*)	M_w (*g/mol*)	PDI
B0	82,935	116,969	1.4
B1	70,594	97,385	1.4
B3	60,553	89,366	1.5
B5	56,209	81,796	1.4
B6	40,922	61,263	1.5

Table 3
Thermal properties of PLA 3D printed samples from the three step DSC.

Batch	T_g (°*C*)	T_m (°*C*)	ΔH_m (*J*/°*C*)
B0	60.5	151.4	2.0
B1	59.2	152.2	4.5
B2	59.1	150.8	28.4
B3	59.8	151.0	28.8
B4	59.2	149.9	30.4
B5	58.8	149.3	32.8
B6	58.6	149.1	32.0

Table 4
Enthalpies values obtained from single ramp DSC tests and degree of crystallinity.

Batch	ΔH_c (J/°C)	ΔH_m (J/°C)	χ (%)
B0	/	32.9	35.4
B1	17.9	30.4	13.3
B2	25.1	30.5	5.8
B3	25.5	29.7	4.5
B4	28.0	33.8	6.2
B5	27.3	31.7	4.8
B6	24.7	31.6	7.4

compared to the virgin material. The value halves after four cycles (B4M), and it further decreases after five cycles (B5M), reducing to −61.4 % from the virgin pellet (B0). The value significantly reduces at the sixth extrusion cycle (B6M), which means −90 %, hence, the material cannot be properly 3D printed after six recycling cycles.

The rheological behavior under typical 3D printing conditions was then evaluated. A feed rate of 20 mm/s was considered the reference feed rate, corresponding to the printing speed selected for the tensile specimens (Table 1). According to Equation (2), the expected shear rate at the internal wall contact of the extruder chamber can be calculated starting from the screw diameter, speed, and channel depth [72]. The expected shear rate in the extrusion chamber is equal to 1.47 s^{-1} at 20 mm/s [79]. The power-law model was used to approximate the curve in the shear rate range of 1–1.9 s^{-1}, using Equation (3). The parameter n gives an overall idea of the behavior of non-Newtonian fluids, where n = 1 corresponds to Newtonian fluids, n < 1 to pseudoplastic fluids (shear-thinning), and n > 1 for dilatant fluids (shear-thickening). According to Table 5, virgin material (B0) has a pseudoplastic behavior, whereas recycled PLA feedstock tends to exhibit a Newtonian-like behavior close to the reference shear rate, almost reaching n = 1 after four and five recycling cycles (B4M and B5M). This fact is also visible in Fig. 4, where the length of the Newtonian plateau increases with the number of recycling processes. In general, the results are consistent with the works from small-scale AM [63], also supported by the decrease in molecular weight analyzed with GPC tests.

3.4. Tensile tests

Tensile tests were performed to analyze the mechanical behavior of recycled PLA feedstock after several extrusion and recycling cycles. The samples exhibited a brittle failure, and their brittleness increased by increasing the number of extrusion and recycling processes. Fig. A4 (Appendix A) shows the stress-strain curves from the tests. Furthermore, the curves are well overlapped for each batch of samples, especially in the initial part, indicating the reproducibility of the results. Table 6 shows the values of elastic modulus (E), ultimate tensile strength (σ_m), fracture strength (σ_b), elongation at maximum stress (ε_m), and elongation at break (ε_b) for 3D printed specimens from one to six extrusion cycles (B1 to B6). The standard deviation is mainly lower than 10 %, also demonstrating the replicability of the data.

Fig. 5a shows the trend of the elastic modulus as a function of the extrusion and recycling processes. After six extrusion cycles (B6), the value of E remains constant, with a minimal decrease of −1.0 %.

Table 5
Zero shear viscosity values from the log-log plots of viscosity and flow index values in the shear rate corresponding to the feed rate at 20 mm/s.

Batch	Extrapolated η0 (Pa·s)	n at $\dot{\gamma}_{print}$ (//)
B0	3641.3	0.69
B1M	2816.6	0.92
B2M	2767.8	0.96
B3M	2082.0	0.99
B4M	1854.7	0.99
B5M	1404.1	0.99
B6M	362.8	0.98

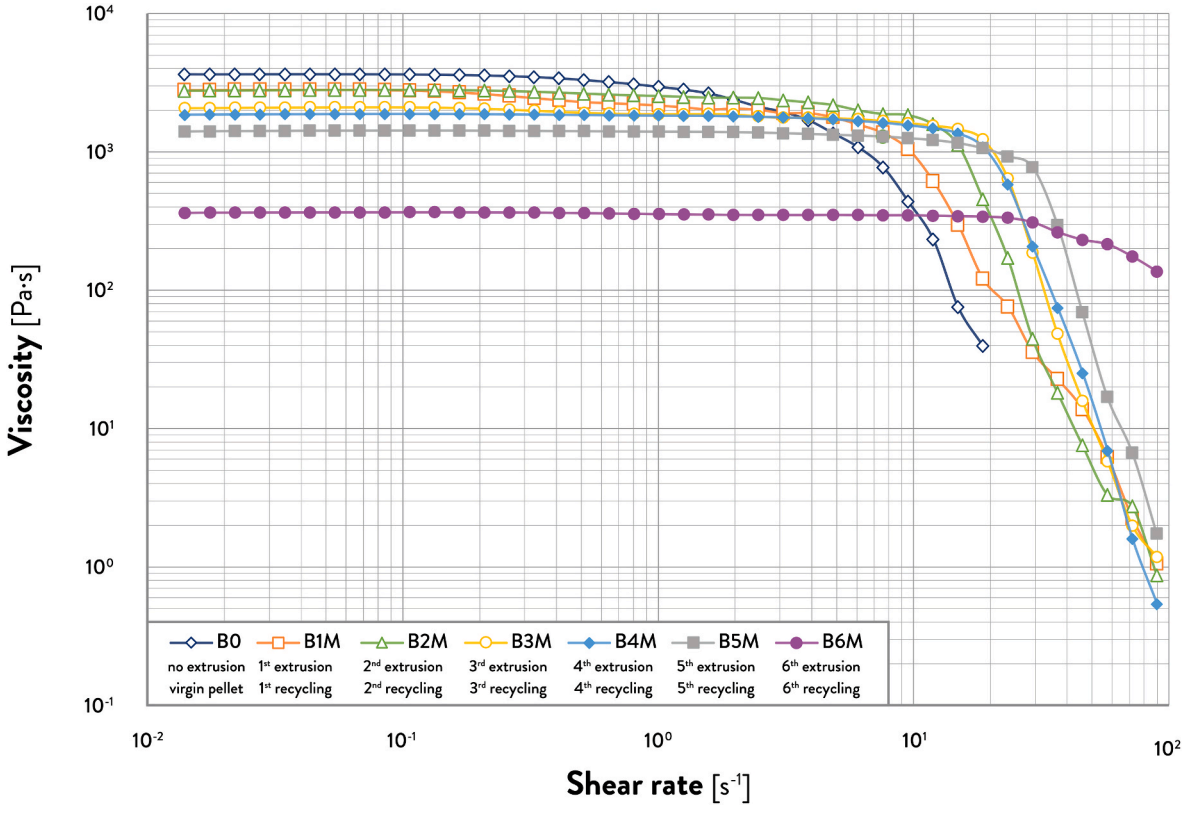

Fig. 4. Log-log plots of viscosity as a function of the shear rate of the PLA feedstock (virgin pellet and shredded feedstock).

Table 6
Values of experimental elastic modulus, ultimate tensile strength, fracture strength, elongation at maximum stress, and elongation at break of the PLA 3D printed batches.

Batch	E (*MPa*)	σ_m (*MPa*)	σ_b (*MPa*)	ε_m (%)	ε_b (%)
B1	3219.6 ± 76.5	62.4 ± 1.7	60.7 ± 1.7	2.4 ± 0.05	2.8 ± 0.18
B2	3418.6 ± 142.0	62.1 ± 1.3	59.9 ± 1.4	2.4 ± 0.15	2.7 ± 0.40
B3	3386.5 ± 43.3	60.1 ± 1.3	59.1 ± 1.2	2.3 ± 0.06	2.4 ± 0.14
B4	3234.6 ± 60.0	57.3 ± 0.6	55.5 ± 1.6	2.3 ± 0.06	2.5 ± 0.14
B5	3280.7 ± 48.0	53.2 ± 2.3	51.5 ± 2.5	1.9 ± 0.17	2.0 ± 0.20
B6	3187.6 ± 68.2	52.2 ± 2.2	51.2 ± 2.3	1.9 ± 0.14	2.0 ± 0.14

However, the average value of E slightly increases (~6 %) after the first and second recycling processes (B2 and B3), with an overlapping of the standard error lines of batches B1 and B2. Similar trends were observed with a small-scale 3D printing system, suggesting the influence of molecular weight reduction on viscosity, improving the interlayer adhesion, and reducing the effect of thermomechanical degradation [62].

The variation of the ultimate tensile strength values exhibited a different trend, as visible from Fig. 5b. The values show a limited variation after the first two recycling cycles (B1 to B3), especially considering the overlapping of the standard error lines. A bigger difference is visible from batch B4, which means after the third recycling cycle, with a decrease of −8.1 % with respect to B1. After the fifth recycling cycle (B6), the value of ultimate tensile strength further decreased by −16.4 %. Despite the significant reduction in molecular weight, ultimate tensile strength seems marginally affected by feedstock degradation, with an overall decrease below 20 %. However, the standard deviation tends to increase, especially for batches B5 and B6, indicating the inhomogeneity of the recycled material used as 3D printing feedstock. The values are comparable to previous work on small-scale 3D printers (~−19 % decrease) [62], despite the influence of the additional extrusion step needed to obtain the filament for each recycling cycle. The trend of the fracture strength (Fig. A5a, Appendix A) is consistent with the ultimate tensile strength values with similar results and percentage reductions after six extrusion cycles (B6), −15.7 %.

According to Fig. 5c, the behavior of elongation at break is similar for batches from B1 to B4, with a significant decrease after four recycling cycles, which means B5 and B6. In this case, the reduction corresponds to −30.1 %, one-third of the initial value of B1. Previous work shows greater decrease of elongation at break after six extrusions [62]. The trends of the elongation at maximum stress (Fig. A5b, Appendix A) and elongation at break are similar, with smaller percentage reductions after six extrusion cycles (B6), −20.5 %.

According to the previous characterization, the decrease in mechanical properties can be mainly affected by the reduction of chain length and average weight molecular weight. As the crystallinity of the PLA feedstock does not increase after each extrusion and recycling process, the variation of the properties is not directly linked to the degree of crystallinity calculated from the DSC tests. Especially for E, the decrease in viscosity can reduce the presence of defects and interlayer voids, partially contrasting the thermomechanical degradation [62]. The direct use of granulate feedstock helps limit the effect of additional extrusion processes on mechanical properties.

3.5. Printability and colorimetric analysis

Different parts were designed and selected to assess the printability of the recycled PLA feedstocks, validating the use of the granulates with feasible geometries with LFAM systems and potentially part of real products. As previously mentioned in Subsection 2.8, two different kinds of samples were fabricated to assess the printability, which means texture samples and demo cut-offs. The former samples aim to compare the printability of the different recycled feedstocks by using the same geometry and the same 3D printing parameters. The latter were used to contextualize the use of LFAM systems and recycled PLA feedstocks in two plausible application fields by investigating different levels of complexity in terms of geometrical features and shapes to be successfully 3D printed.

Focusing on the first printability test (texture samples), a specific sample was designed and 3D printed by using different batches of material (Fig. 6a). The 3D model has a revolution-like shape with an embossed and engraved surface. The diamond-textured surface reaches a maximum overhang of 30°, and it allows to qualitatively assess the quality of the 3D printing process by checking the dimensional accuracy of the texture surface and any possible defect from the 3D printing process. This sample was initially 3D printed with the virgin pellet (B0) to define a set of optimal parameters for the test, which was also used as a benchmark for the comparison with the parts fabricated with the recycled feedstock. As visible in Fig. 6b, several defects and inhomogeneities were observed in the first 3D printed sample, processed at a feed rate of 20 mm/s. Moreover, the sharp corners of the diamond-textured surface and its overhangs highlighted some critical issues in terms of dimensional accuracy, leading to partial collapses in specific points, i.e., overhangs at the maximum peaks of emboss and engraves (circled in red in Fig. 6b). These defects were mainly attributed to the small cross-section layer areas of the part, reducing the cooling down times for each layer before the deposition of the following one [41,42]. The printing speed was therefore reduced to 8 mm/s to fabricate the benchmark sample from virgin pellets (B1, Fig. 6c), also refining the parameters for the test resumed in Table 1.

Fig. 7 shows the 3D printed samples with the virgin pellet (B0, on the

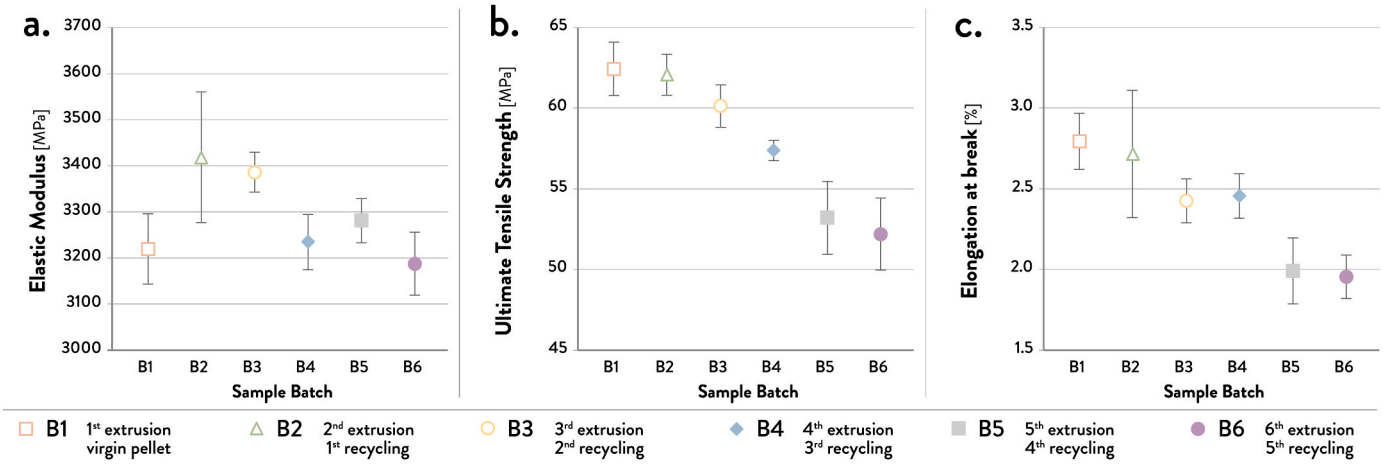

Fig. 5. Comparison of the experimental values from the tensile tests: (a) elastic modulus, (b) ultimate tensile strength, and (c) elongation at break.

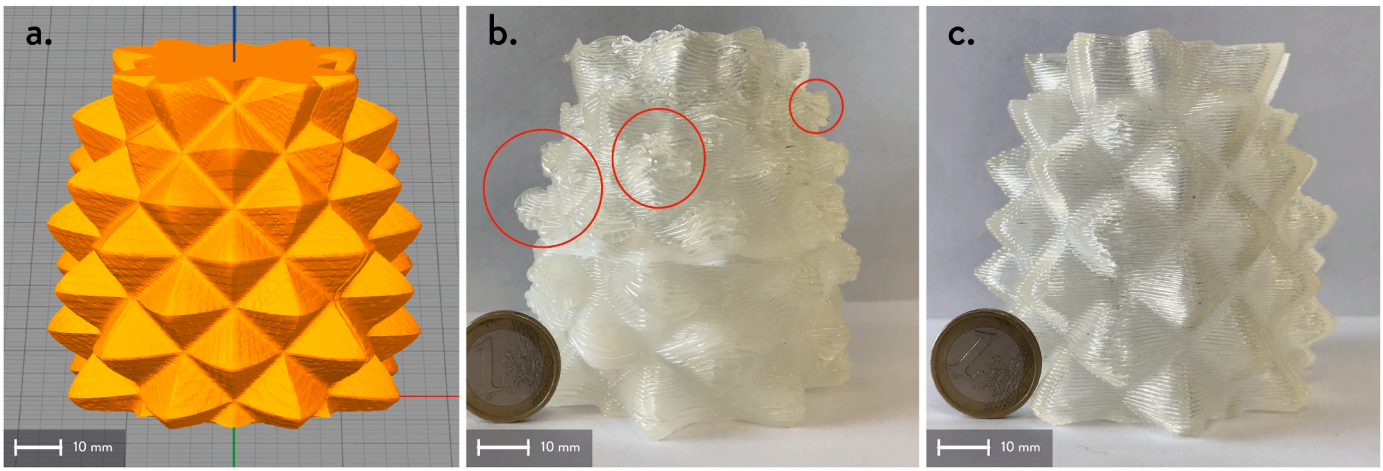

Fig. 6. Texture sample: (a) 3D model, (b) preliminary trial printed at 20 mm/s with some defects (circled in red), and (c) trial at 8 mm/s without surface defects. (For interpretation of the references to color in this figure legend, the reader is referred to the Web version of this article.)

left) and the different recycled PLA feedstock (B1 to B6). In general, the quality of the parts is quite consistent, and the diamond-textured surface is distinguishable after multiple extrusion and recycling processes. Some minor inaccuracies can be seen in the lower part of the samples from B4 to B6, corresponding to the overhangs of 30°. This issue can be linked to the decrease in viscosity that emerged from the rheological tests, affecting the shape retention of the extruded path before its complete cooling down. However, a noticeable difference was observed in colors, ranging from the transparent-like hue of virgin pellets to a yellowish or brownish hue after multiple cycles.

A colorimetric analysis was performed to quantify the color variation after each extrusion and recycling process. As shown in Table 7, sample B1 produced with virgin pellets has a relatively neutral color, as indicated by the values of a* and b*, and a tendency to lightness (high value of L*). A noticeable color variation was observed starting from sample B2, with high values of discoloration (ΔE*). In detail, the color shifted toward yellow (increase in b*) and became darker (decrease in L*). However, these color changes remained consistent across the different samples, as visible from the direction of the color difference, especially ΔL* and Δb* (~2 units). This color variation is in line with the previous thermal analysis from DSC, indicating the thermomechanical degradation of the material after several cycles. The increase in yellowness also confirms the GPC analysis, indicating a molecular weight decrease [62,64].

Some demo parts were 3D printed as a proof-of-concept of possible applications with the recycled PLA feedstocks analyzed in this work, trying to envision new real-world exploitations. The number of new applications with 3D printed recycled materials has progressively

Table 7
Mean CIELAB L*, a*, b* values, ΔL*, Δa*, Δb* (direction of the color difference), and ΔE* (discoloration) of the different 3D printed sample batches.

Sample	L*	a*	b*	ΔL*	Δa*	Δb*	ΔE*
B1	67.72 ± 0.84	−0.09 ± 0.09	7.62 ± 0.21	//	//	//	//
B2	57.41 ± 0.42	−0.28 ± 0.17	17.59 ± 2.01	−10.32	−0.19	9.97	14.35
B3	57.47 ± 0.72	0.37 ± 0.11	16.78 ± 1.34	−10.26	0.46	9.13	13.74
B4	56.37 ± 0.56	0.27 ± 0.21	17.69 ± 0.69	−11.36	0.36	10.07	15.18
B5	56.12 ± 1.07	0.12 ± 0.14	17.46 ± 0.17	−11.6	0.21	9.84	15.21
B6	54.27 ± 1.14	0.36 ± 0.06	16.24 ± 0.56	−13.44	0.45	8.63	15.98

increased in the last few years [29,30,43], requiring a more systematic approach to material characterization and further investigation with large-format FGF systems. As visible in Fig. 8, two different applications were selected as case studies for the demonstration. The two sectors and the specific product typology were chosen by considering an increasing level of geometrical complexity to be achieved and the results from the materials characterization of the recycled feedstocks. The first case study is linked to the furniture sector and uses recycled PLA feedstock to fabricate customized elements designed for LFAM, such as modular chairs, stools, or tables for stands and exhibitions [80]. The cut-offs shown in Fig. 8a represent some joints to connect the different structural elements, requiring good printing accuracy and mechanical

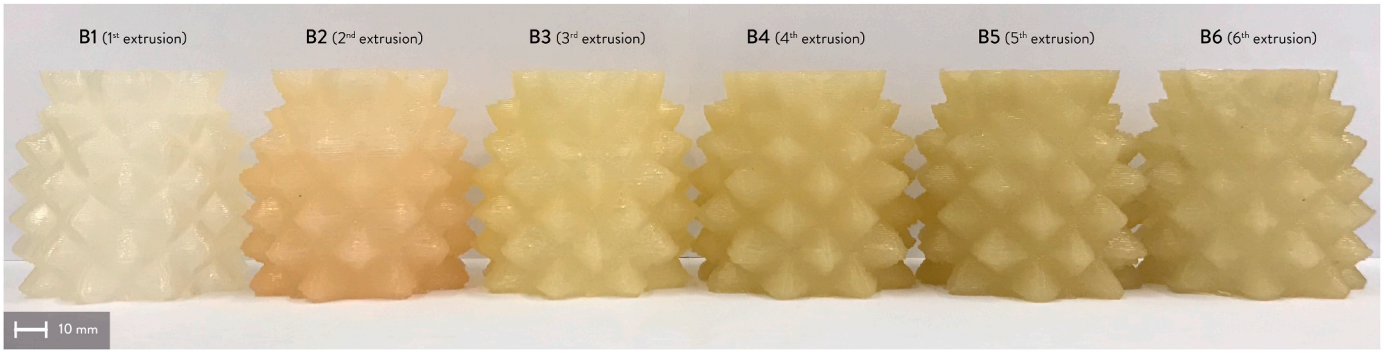

Fig. 7. Texture samples 3D printed with the different batches of PLA feedstock (from left to right): first (virgin pellet, B1), second (B2), third (B3), fourth (B4), fifth (B5) and sixth (B6) extrusion cycle through 3D printing.

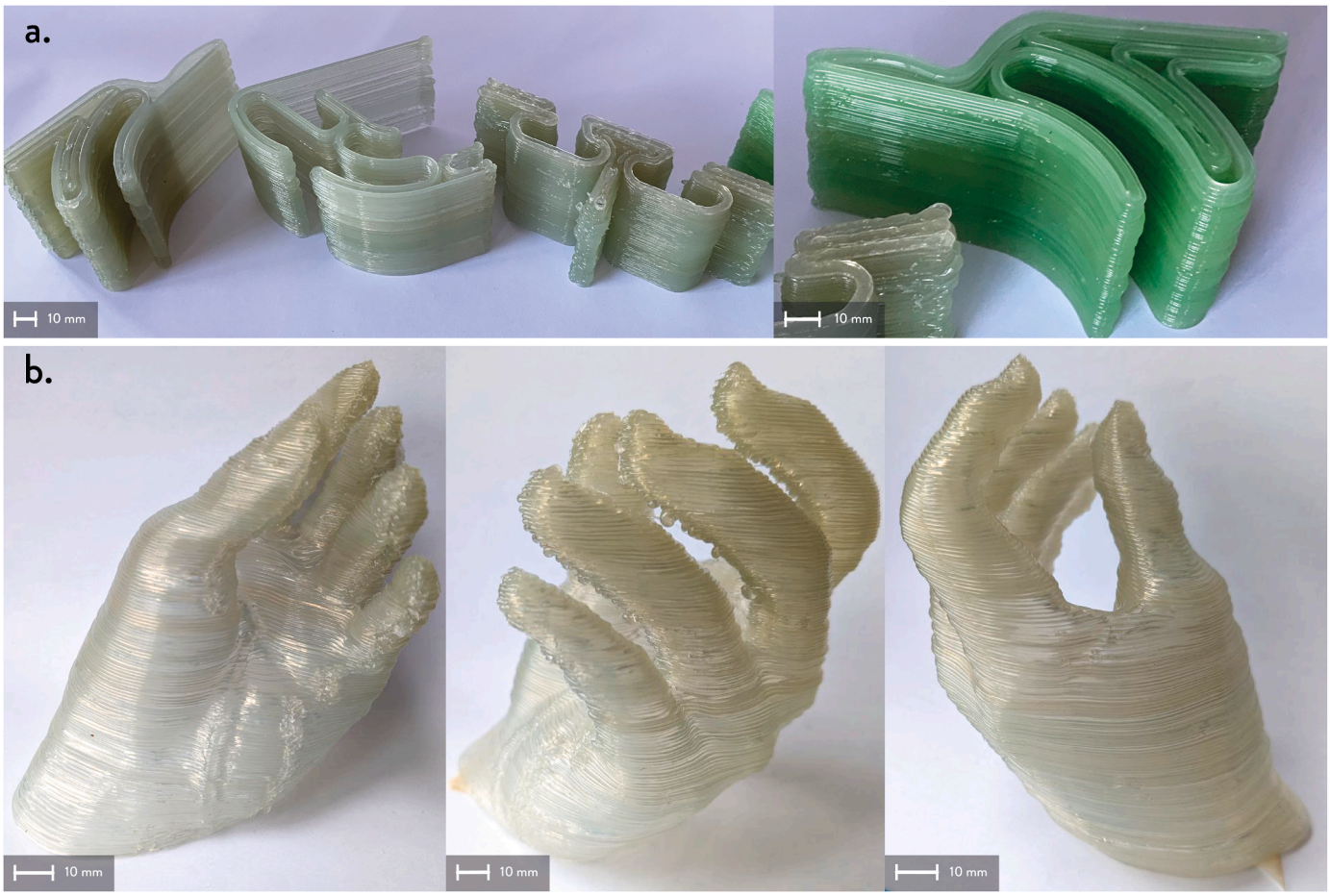

Fig. 8. Demo cut-offs from application case studies: (a) joint cut-offs from furniture elements (modular chairs, tables, and stools) printed with B1M (left) and B3M (right), and (b) complex shape cut-off of art replicas printed with B1M.

properties to meet the design requirements. Different parts were 3D printed with feedstock B1M, which means after one recycling cycle. According to Table 1, different layer heights were selected for the different trials, i.e., 0.5, 0.7, and 1 mm. Feedstock B3M was also successfully used to fabricate some joints, which means using recycled PLA feedstock after three recycling cycles.

The second case study wants to demonstrate the feasibility of complex freeform shapes with recycled feedstock. The selected 3D model is a cut-off from large-format art replicas, originally reaching an overall height of 2 m. A first part was initially fabricated with the virgin PLA pellet (B0) to ensure the feasibility of the selected cut-off with a LFAM 3D printer, especially of the most challenging geometrical features, e.g., self-standing overhangs, small features compared to the nozzle dimension, and small discontinued cross-sections to be 3D printed (Fig. A6, Appendix A). The part was then successfully 3D printed with feedstock B1M, reaching a good printing accuracy and shape retention of the overhangs and small sections (Fig. 8b) compared to the benchmark test with the virgin granulates (Fig. A6). In this case, using feedstock B3M resulted in failures during the 3D printing process, mainly linked to the decreased viscosity and multiple collapses of the previous layers during the cooling down. However, the results are promising, especially considering the dimensions of the samples. Cooling down-related issues could be solved by fabricating parts with bigger cross-sectional areas, increasing the cooling down times for each layer and reaching the typical building volumes of large-format AM processes [36,37].

The printability tests mainly focused on small parts with complex detailed geometries considering the dimension of the selected nozzle diameter (3 mm). Although LFAM systems are generally used for bigger pieces, this choice increased the complexity of obtaining the 3D printed demo cut-offs, fabricating samples with significantly small cross-sections for each layer, hence low cooling times considering LFAM systems equipped with big nozzle diameters [41,42]. This fact exacerbates the risk of deformations and collapses, as well as using typical nozzle diameters for LFAM systems, which usually range from 2 to 10 mm [37]. Therefore, the results achieved in this work can foster the use of similar recycled PLA granular feedstock to fabricate big objects with optimized cross-section dimensions and cooling times. For instance, other recycled PLA granulates comparable to B1M feedstock have been used by one of the authors as a secondary raw material for real furniture products, e.g., stools, using the same LFAM FGF 3D printing system and recycling procedure of this work [81]. This fact represents a starting point to validate the use of these recycled granulates within new real-world contexts, also using feedstock after multiple recycling processes.

4. Conclusions

This paper investigated the thermal, rheological, and mechanical behavior of PLA granulate feedstock after multiple 3D printing and recycling processes with a LFAM system. Six extrusion and recycling cycles were assessed during the characterization. The effect of thermo-mechanical degradation on molecular weight and thermal properties after multiple cycles was assessed thanks to GPC and DSC analyses. The processing conditions in the extruder chamber were simulated during a flow stress ramp test to study the rheological behavior of the different recycled PLA feedstock. Tensile tests were performed to evaluate the

influence of the multiple reprocessing cycles on the mechanical properties. Some samples were 3D printed to assess the overall quality and perform a colorimetry test. Using recycled PLA feedstock for potential applications was then demonstrated through cut-offs and complex geometries from demo applications.

Despite the decrease in molecular weight, granulate recycled PLA feedstock processed with LFAM FGF is less affected by thermomechanical degradation than desktop-size FFF systems by avoiding further reprocessing steps on secondary raw materials, i.e., extruding filaments. Except for the enthalpy of fusion, thermal properties exhibited minor variations after multiple cycles. The material is mainly amorphous, showing a constant degree of crystallinity linked to the homogeneous distribution of molecular weights. According to the decrease in molecular weight, viscosity values significantly decrease, especially after six recycling cycles, with a tendency to Newtonian-like behavior at a shear rate corresponding to average feed rates. The direct extrusion of recycled granulate feedstock and the decrease in viscosity limited the effect of the thermomechanical degradation on the mechanical properties, especially for the elastic modulus. Despite the increase in yellowness, good printability was achieved by fabricating 3D printed parts for possible applications in the furniture and exhibition sectors after a maximum of three cycles.

Recycled PLA feedstock on large-Format FGF 3D printers represents a viable alternative to virgin pellets, scaling up the recycling process by cutting the reprocessing steps to obtain new filaments for desktop-size 3D printers. In general, using recycled granular feedstock on LFAM FGF systems reduces the thermomechanical degradation of the secondary raw material, as well as the energy consumption and environmental impact of its reprocessing. Simple large-scale components can be manufactured with recycled PLA feedstock until five recycling processes, whereas feedstock until three recycling cycles may be used for complex geometries and structural applications. This work represents a guideline for designers and engineers interested in implementing LFAM FGF systems and recycled feedstocks in their professional activity. It resumes the main information to consider for designing new products and applications, and it can stimulate researchers to investigate the use of different materials with similar 3D printing systems. In addition, studying multiple recycling can support professionals in adopting a more comprehensive perspective with AM technologies, going beyond the first end-of-life of a product when designing new applications, i.e., from cradle to cradle. Further studies should investigate alternative feedstock for new fully bio-based materials, i.e., using recycled PLA as a matrix for composites filled with biomass waste, and evaluate different 3D printing systems, including more accessible equipment, such as open source 3D printers. Bigger parts can also be fabricated to deepen the analysis from the printability tests, further validating the results from the 3D printed demo cut-offs. In addition, other characterization analyses can also be performed to further support practitioners in exploiting similar materials, such as impact or flexural tests and other morphological fracture analyses. Finally, sustainability metrics and LCA should be used to validate their use in specific real-world contexts by evaluating the environmental impacts, fostering collaborations to develop new products and applications.

Declaration of competing interest

The authors declare that they have no known competing financial interests or personal relationships that could have appeared to influence the work reported in this paper.

Data availability

Data will be made available on request.

Acknowledgements

The authors would like to acknowledge Juan Sebastian Barrera Cely for providing the 3D models of the furniture elements used as first application case study. This research received no external fundings.

Appendix A. PLA Characterization graphs

A.1. GPC

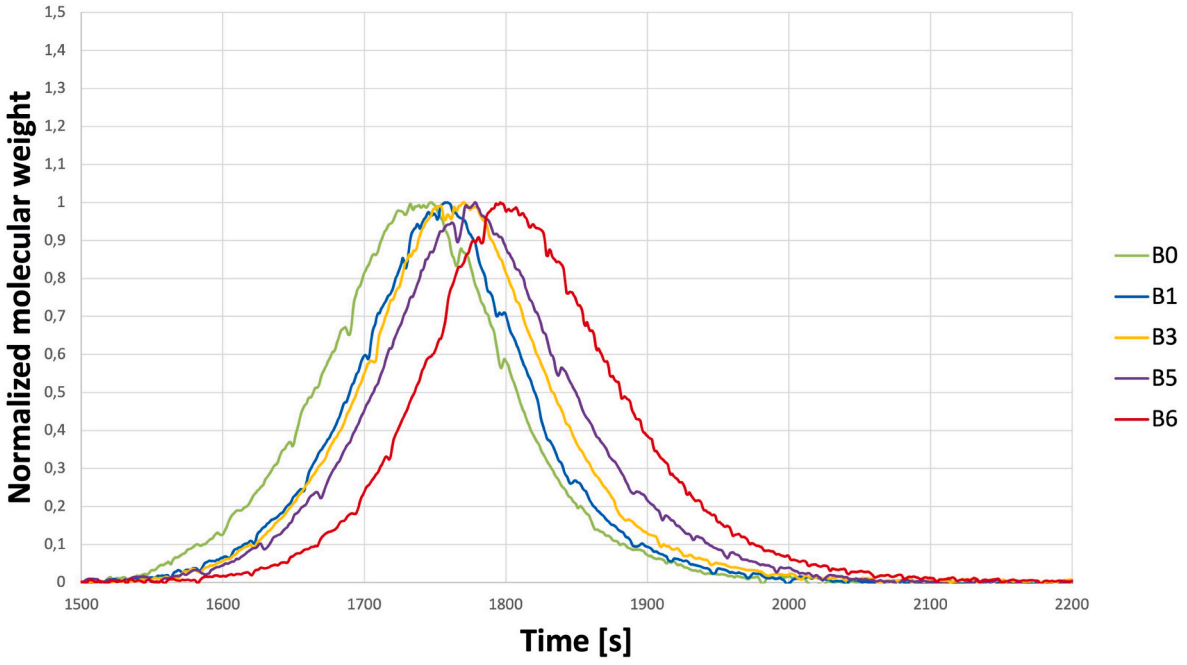

Fig. A1. Molecular weight distribution curves of PLA feedstock from GPC tests of samples B0, B1, B3, B5, and B6.

A.2. DSC

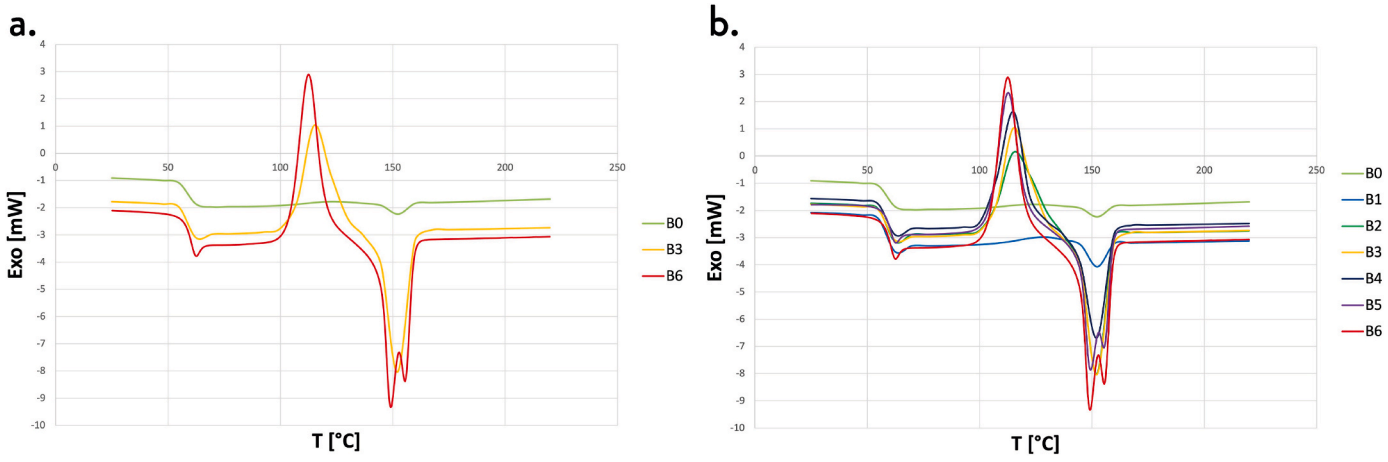

Fig. A2. Comparison of the DSC curves of: (a) second ramp of B0, B3, and B6; and (b) second ramp from B0 to B6.

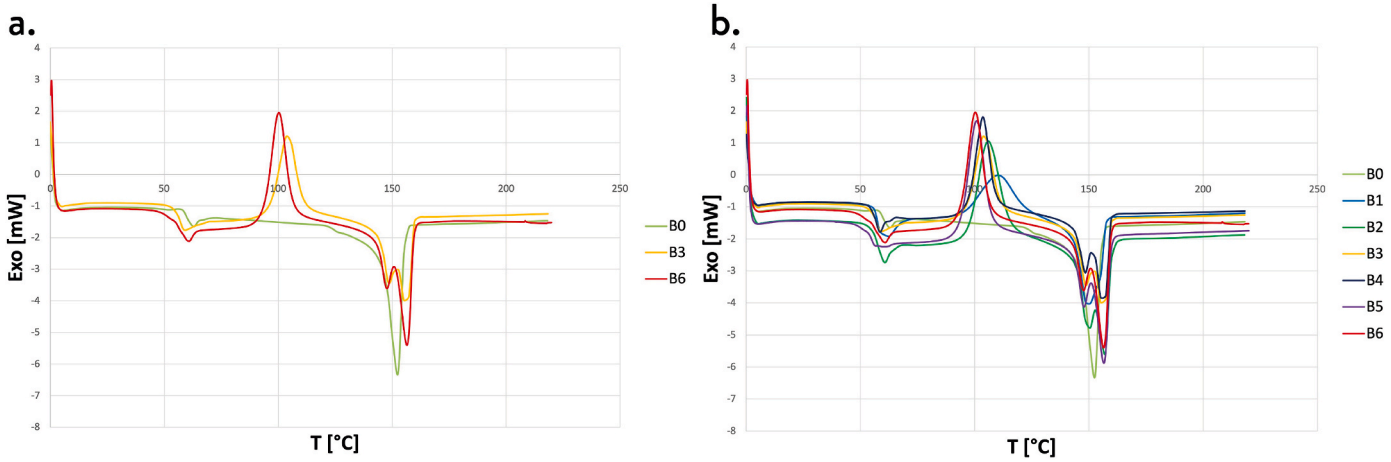

Fig. A3. Comparison of the DSC curves of: (a) single ramp of B0, B3, and B6; and (b) single ramp from B0 to B6.

A.3. Tensile tests

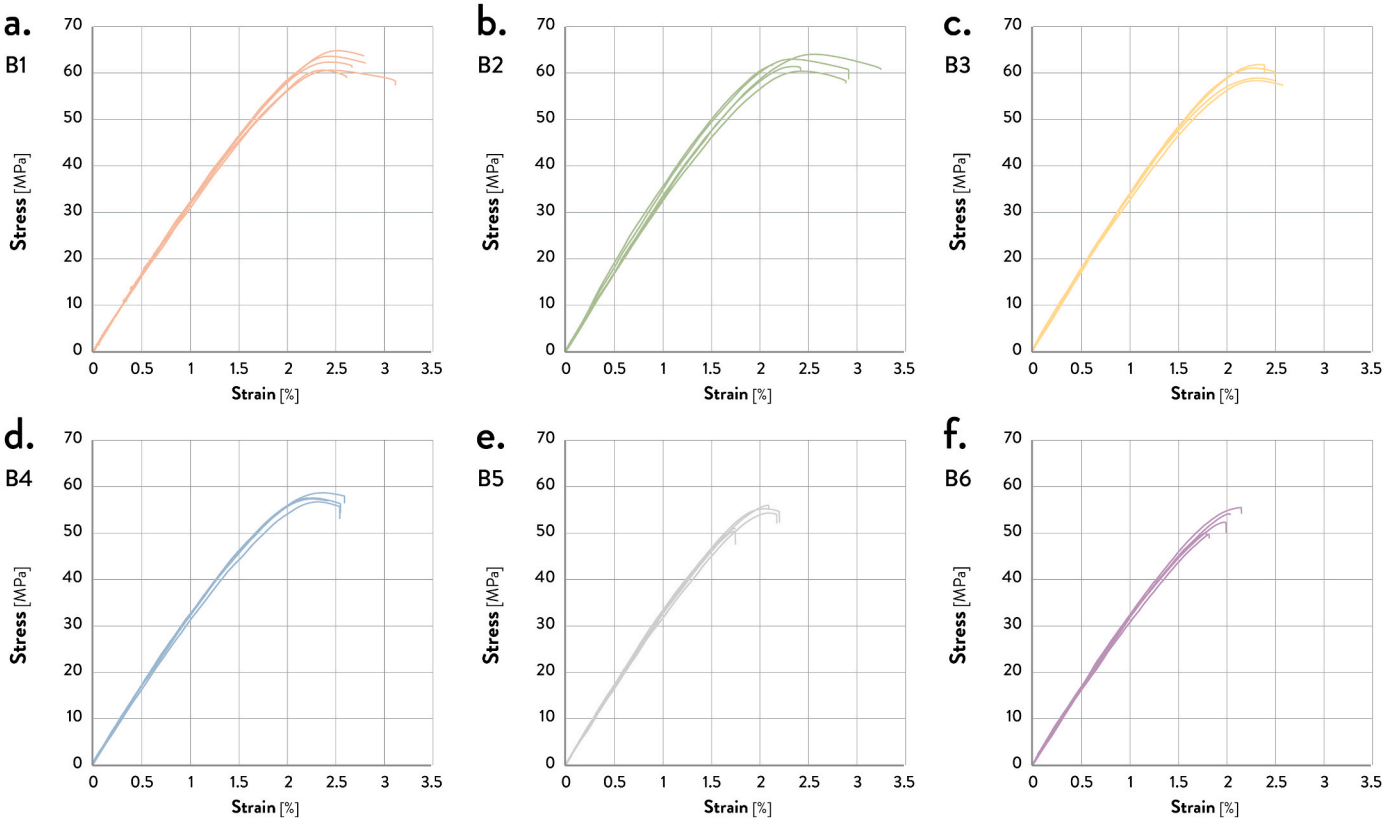

Fig. A4. Stress-strain curves from the different batches of tensile specimens: (a) B1; (b) B2; (c) B3; (d) B4; (e) B5; and (f) B6.

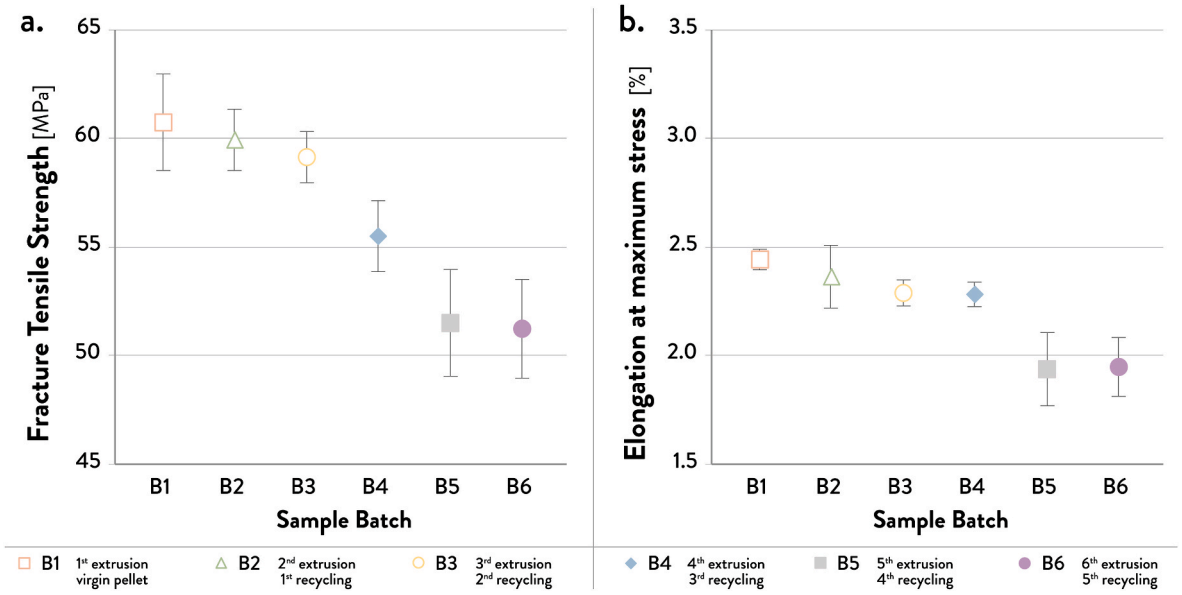

Fig. A5. Comparison of the experimental values from the tensile tests: (a) fracture strength and (b) elongation at maximum stress.

A.4. Cut-off benchmark with 3D printed virgin PLA pellet

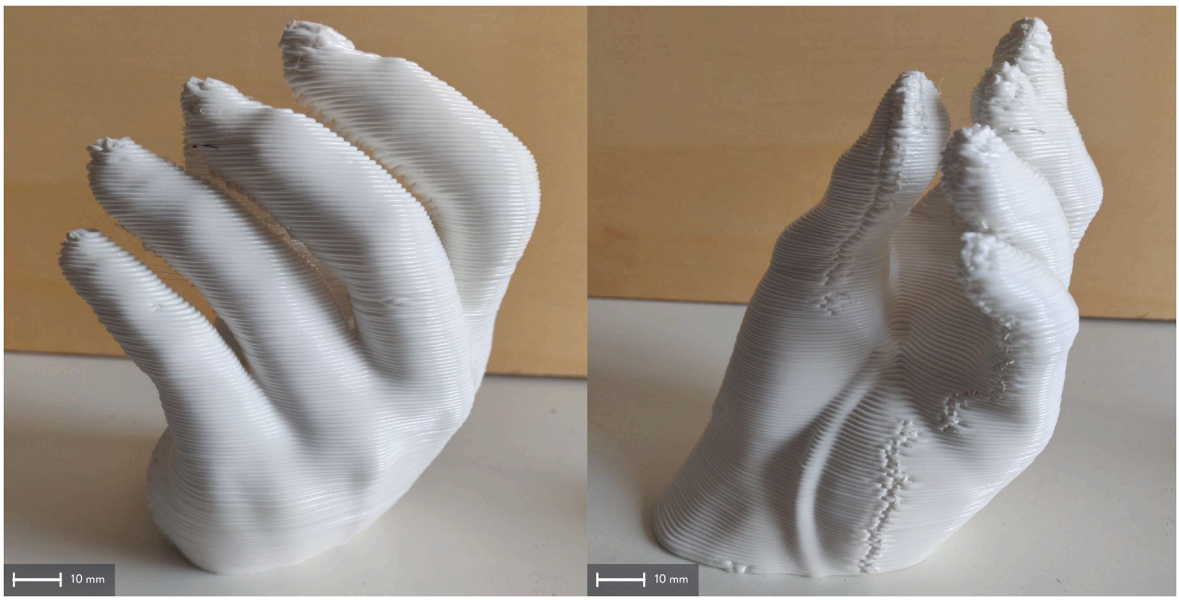

Fig. A6. Demo cut-off of the art replica 3D printed with virgin PLA pellets (B0), used as a benchmark for the recycled PLA feedstock.

References

[1] A.D. Jayal, F. Badurdeen, O.W. Dillon, I.S. Jawahir, Sustainable manufacturing: modeling and optimization challenges at the product, process and system levels, CIRP J. Manuf. Sci. Technol. 2 (2010) 144–152, https://doi.org/10.1016/j.cirpj.2010.03.006.

[2] R. Greer, T. von Wirth, D. Loorbach, The Waste-Resource Paradox: practical dilemmas and societal implications in the transition to a circular economy, J. Clean. Prod. 303 (2021), https://doi.org/10.1016/j.jclepro.2021.126831.

[3] P. Saxena, P. Stavropoulos, J. Kechagias, K. Salonitis, Sustainability assessment for manufacturing operations, Energies 13 (2020) 2730, https://doi.org/10.3390/en13112730.

[4] C. Grabowik, K. Kalinowski, Z. Monica, Integration of the CAD/CAPP/PPC systems, J. Mater. Process. Technol. 164–165 (2005) 1358–1368, https://doi.org/10.1016/j.jmatprotec.2005.02.036.

[5] A. Diaz, J.-P. Schöggl, T. Reyes, R.J. Baumgartner, Sustainable product development in a circular economy: implications for products, actors, decision-making support and lifecycle information management, Sustain. Prod. Consum. 26 (2021) 1031–1045, https://doi.org/10.1016/j.spc.2020.12.044.

[6] A. dos Santos, C. Vezzoli, B. Garcia Parra, S. Molina Mata, S. Banerjee, C. Kohtala, et al., Distributed economies, in: C. Vezzoli, B. Garcia Parra, C. Kohtala (Eds.), Designing Sustainability for All: the Design of Sustainable Product-Service Systems Applied to Distributed Economies, Springer International Publishing, Cham, 2021, pp. 23–50, https://doi.org/10.1007/978-3-030-66300-1_2.

[7] B. Corona, L. Shen, D. Reike, J. Rosales Carreón, E. Worrell, Towards sustainable development through the circular economy—a review and critical assessment on current circularity metrics, Resour. Conserv. Recycl. 151 (2019), 104498, https://doi.org/10.1016/j.resconrec.2019.104498.

[8] M. Geissdoerfer, P. Savaget, N.M.P. Bocken, E.J. Hultink, The Circular Economy – a new sustainability paradigm? J. Clean. Prod. 143 (2017) 757–768, https://doi.org/10.1016/j.jclepro.2016.12.048.

[9] Ellen MacArthur Foundation (Emf), Towards the Circular Economy, 2013.
[10] P. Ghisellini, C. Cialani, S. Ulgiati, A review on circular economy: the expected transition to a balanced interplay of environmental and economic systems, J. Clean. Prod. 114 (2016) 11–32, https://doi.org/10.1016/j.jclepro.2015.09.007.
[11] K. Campbell-Johnston, W.J.V. Vermeulen, D. Reike, S. Brullot, The circular economy and cascading: towards a framework, Resour. Conserv. Recycl. 7 (2020), 100038, https://doi.org/10.1016/j.rcrx.2020.100038.
[12] K. Winans, A. Kendall, H. Deng, The history and current applications of the circular economy concept, Renew. Sustain. Energy Rev. 68 (2017) 825–833, https://doi.org/10.1016/j.rser.2016.09.123.
[13] X. Zhao, M. Korey, K. Li, K. Copenhaver, H. Tekinalp, S. Celik, et al., Plastic waste upcycling toward a circular economy, Chem. Eng. J. 428 (2022), 131928, https://doi.org/10.1016/j.cej.2021.131928.
[14] M.F. Ashby, Chapter 14 - the vision: a circular materials economy, in: M.F. Ashby (Ed.), Materials and Sustainable Development, Butterworth-Heinemann, Boston, 2016, pp. 211–239, https://doi.org/10.1016/B978-0-08-100176-9.00014-1.
[15] J. Zheng, S. Suh, Strategies to reduce the global carbon footprint of plastics, Nat. Clim. Change 9 (2019) 374–378, https://doi.org/10.1038/s41558-019-0459-z.
[16] Recycling and the future of the plastics industry | McKinsey n.d. https://www.mckinsey.com/industries/chemicals/our-insights/how-plastics-waste-recycling-could-transform-the-chemical-industry (accessed June 30, 2023).
[17] World Economic Forum the New Plastics Economy—Rethinking the Future of Plastics, Ellen MacArthur Foundation, McKinsey & Company, 2016.
[18] D. Calleja, Why the "New Plastics Economy" must be a circular economy, Field Actions Sci. Reports The J. Field Actions (2019) 22–27.
[19] M.E. Grigore, Methods of recycling, properties and applications of recycled thermoplastic polymers, Recycling 2 (2017) 24, https://doi.org/10.3390/recycling2040024.
[20] N. Singh, D. Hui, R. Singh, I.P.S. Ahuja, L. Feo, F. Fraternali, Recycling of plastic solid waste: a state of art review and future applications, Compos. B Eng. 115 (2017) 409–422, https://doi.org/10.1016/j.compositesb.2016.09.013.
[21] W. d'Ambrières, Plastics recycling worldwide: current overview and desirable changes, Field Actions Sci. Reports The J. Field Actions (2019) 12–21.
[22] L.F. Dumée, Circular materials and circular design—review on challenges towards sustainable manufacturing and recycling, CircEconSust 2 (2022) 9–23, https://doi.org/10.1007/s43615-021-00085-2.
[23] D. Sumter, J. de Koning, C. Bakker, R. Balkenende, Key competencies for design in a circular economy: exploring gaps in design knowledge and skills for a circular economy, Sustainability 13 (2021) 776, https://doi.org/10.3390/su13020776.
[24] M. Despeisse, M. Baumers, P. Brown, F. Charnley, S.J. Ford, A. Garmulewicz, et al., Unlocking value for a circular economy through 3D printing: a research agenda, Technol. Forecast. Soc. Change 115 (2017) 75–84, https://doi.org/10.1016/j.techfore.2016.09.021.
[25] T.M. Tavares, G.M.D. Ganga, M. Godinho Filho, V.P. Rodrigues, The benefits and barriers of additive manufacturing for circular economy: a framework proposal, Sustain. Prod. Consum. 37 (2023) 369–388, https://doi.org/10.1016/j.spc.2023.03.006.
[26] M.R. Khosravani, T. Reinicke, On the environmental impacts of 3D printing technology, Appl. Mater. Today 20 (2020), 100689, https://doi.org/10.1016/j.apmt.2020.100689.
[27] M. Garg, R. Rani, V.K. Meena, S. Singh, Significance of 3D printing for a sustainable environment, Mater. Today Sustain. (2023), 100419, https://doi.org/10.1016/j.mtsust.2023.100419.
[28] I. Gibson, D. Rosen, B. Stucker, M. Khorasani, Additive Manufacturing Technologies, Springer International Publishing, Cham, 2021, https://doi.org/10.1007/978-3-030-56127-7.
[29] K. Mikula, D. Skrzypczak, G. Izydorczyk, J. Warchoł, K. Moustakas, K. Chojnacka, et al., 3D printing filament as a second life of waste plastics—a review, Environ. Sci. Pollut. Res. 28 (2021) 12321–12333, https://doi.org/10.1007/s11356-020-10657-8.
[30] F.A. Cruz Sanchez, H. Boudaoud, M. Camargo, J.M. Pearce, Plastic recycling in additive manufacturing: a systematic literature review and opportunities for the circular economy, J. Clean. Prod. 264 (2020), 121602, https://doi.org/10.1016/j.jclepro.2020.121602.
[31] ASTM International, ISO/ASTM 52900-15 Standard Terminology for Additive Manufacturing – General Principles – Terminology, ASTM International, West Conshohocken, PA, 2015.
[32] S.C. Ligon, R. Liska, J. Stampfl, M. Gurr, R. Mülhaupt, Polymers for 3D printing and customized additive manufacturing, Chem. Rev. 117 (2017) 10212–10290, https://doi.org/10.1021/acs.chemrev.7b00074.
[33] J. Huang, Q. Chen, H. Jiang, B. Zou, L. Li, J. Liu, et al., A survey of design methods for material extrusion polymer 3D printing, Virtual Phys. Prototyp. 15 (2020) 148–162, https://doi.org/10.1080/17452759.2019.1708027.
[34] E.U. Enemuoh, V.G. Menta, A. Abutunis, S. O'Brien, L.I. Kaya, J. Rapinac, Energy and eco-impact evaluation of fused deposition modeling and injection molding of polylactic acid, Sustainability 13 (2021) 1875, https://doi.org/10.3390/su13041875.
[35] J. Kechagias, D. Chaidas, Fused filament fabrication parameter adjustments for sustainable 3D printing, Mater. Manuf. Process. 38 (2023) 933–940, https://doi.org/10.1080/10426914.2023.2176872.
[36] H. Al Jassmi, F. Al Najjar, A.-H.I. Mourad, Large-scale 3D printing: the way forward, IOP Conf. Ser. Mater. Sci. Eng. 324 (2018), 012088, https://doi.org/10.1088/1757-899X/324/1/012088.
[37] D. Moreno Nieto, V. Casal López, S.I. Molina, Large-format polymeric pellet-based additive manufacturing for the naval industry, Addit. Manuf. 23 (2018) 79–85, https://doi.org/10.1016/j.addma.2018.07.012.
[38] F. Pignatelli, G. Percoco, An application- and market-oriented review on large format additive manufacturing, focusing on polymer pellet-based 3D printing, Prog. Addit. Manuf. (2022), https://doi.org/10.1007/s40964-022-00309-3.
[39] P. Chesser, B. Post, A. Roschli, C. Carnal, R. Lind, M. Borish, et al., Extrusion control for high quality printing on Big Area Additive Manufacturing (BAAM) systems, Addit. Manuf. 28 (2019) 445–455, https://doi.org/10.1016/j.addma.2019.05.020.
[40] V. Kishore, C. Ajinjeru, A. Nycz, B. Post, J. Lindahl, V. Kunc, et al., Infrared preheating to improve interlayer strength of big area additive manufacturing (BAAM) components, Addit. Manuf. 14 (2017) 7–12, https://doi.org/10.1016/j.addma.2016.11.008.
[41] E. Meraz Trejo, X. Jimenez, K.M.M. Billah, J. Seppala, R. Wicker, D. Espalin, Compressive deformation analysis of large area pellet-fed material extrusion 3D printed parts in relation to in situ thermal imaging, Addit. Manuf. 33 (2020), 101099, https://doi.org/10.1016/j.addma.2020.101099.
[42] T. D'Amico, A.M. Peterson, Bead parameterization of desktop and room-scale material extrusion additive manufacturing: how print speed and thermal properties affect heat transfer, Addit. Manuf. 34 (2020), 101239, https://doi.org/10.1016/j.addma.2020.101239.
[43] A. Romani, V. Rognoli, M. Levi, Design, materials, and extrusion-based additive manufacturing in circular economy contexts: from waste to new products, Sustainability 13 (2021) 7269, https://doi.org/10.3390/su13137269.
[44] A. Romani, R. Suriano, M. Levi, Biomass waste materials through extrusion-based additive manufacturing: a systematic literature review, J. Clean. Prod. 386 (2023), 135779, https://doi.org/10.1016/j.jclepro.2022.135779.
[45] S. Bhagia, K. Bornani, R. Agrawal, A. Satlewal, J. Ďurkovič, R. Lagaňa, et al., Critical review of FDM 3D printing of PLA biocomposites filled with biomass resources, characterization, biodegradability, upcycling and opportunities for biorefineries, Appl. Mater. Today 24 (2021), 101078, https://doi.org/10.1016/j.apmt.2021.101078.
[46] M. Kreiger, G.C. Anzalone, M.L. Mulder, A. Glover, J.M. Pearce, Distributed recycling of post-consumer plastic waste in rural areas, MRS Proc. 1492 (2013) 91–96, https://doi.org/10.1557/opl.2013.258.
[47] A.O. Laplume, B. Petersen, J.M. Pearce, Global value chains from a 3D printing perspective, J. Int. Bus. Stud. 47 (2016) 595–609, https://doi.org/10.1057/jibs.2015.47.
[48] M.A. Kreiger, M.L. Mulder, A.G. Glover, J.M. Pearce, Life cycle analysis of distributed recycling of post-consumer high density polyethylene for 3-D printing filament, J. Clean. Prod. 70 (2014) 90–96, https://doi.org/10.1016/j.jclepro.2014.02.009.
[49] R.S. Rattan, N. Nauta, A. Romani, J.M. Pearce, Hangprinter for large scale additive manufacturing using fused particle fabrication with recycled plastic and continuous feeding, HardwareX 13 (2023), e00401, https://doi.org/10.1016/j.ohx.2023.e00401.
[50] A. Petsiuk, B. Lavu, R. Dick, J.M. Pearce, Waste plastic direct extrusion hangprinter, Inventions 7 (2022) 70, https://doi.org/10.3390/inventions7030070.
[51] M.J. Reich, A.L. Woern, N.G. Tanikella, J.M. Pearce, Mechanical properties and applications of recycled polycarbonate particle material extrusion-based additive manufacturing, Materials 12 (2019) 1642, https://doi.org/10.3390/ma12101642.
[52] W.L. Hawkins, Polymer degradation, in: W.L. Hawkins (Ed.), Polymer Degradation and Stabilization, Springer, Berlin, Heidelberg, 1984, pp. 3–34, https://doi.org/10.1007/978-3-642-69376-2_2.
[53] K. Pielichowski, J. Njuguna, T.M. Majka, 2 - mechanisms of thermal degradation of polymers, in: K. Pielichowski, J. Njuguna, T.M. Majka (Eds.), Thermal Degradation of Polymeric Materials, second ed., Elsevier, 2023, pp. 9–11, https://doi.org/10.1016/B978-0-12-823023-7.00001-0.
[54] F. Signori, M.-B. Coltelli, S. Bronco, Thermal degradation of poly(lactic acid) (PLA) and poly(butylene adipate-co-terephthalate) (PBAT) and their blends upon melt processing, Polym. Degrad. Stabil. 94 (2009) 74–82, https://doi.org/10.1016/j.polymdegradstab.2008.10.004.
[55] F.-D. Kopinke, M. Remmler, K. Mackenzie, M. Möder, O. Wachsen, Thermal decomposition of biodegradable polyesters—II. Poly(lactic acid), Polym. Degrad. Stabil. 53 (1996) 329–342, https://doi.org/10.1016/0141-3910(96)00102-4.
[56] T.D. Ngo, A. Kashani, G. Imbalzano, K.T.Q. Nguyen, D. Hui, Additive manufacturing (3D printing): a review of materials, methods, applications and challenges, Composites, Part B 143 (2018) 172–196, https://doi.org/10.1016/j.compositesb.2018.02.012.
[57] V. Gil Muñoz, L.M. Muneta, R. Carrasco-Gallego, J. de Juanes Marquez, D. Hidalgo-Carvajal, Evaluation of the circularity of recycled PLA filaments for 3D printers, Appl. Sci. 10 (2020) 8967, https://doi.org/10.3390/app10248967.
[58] C. Abeykoon, P. Sri-Amphorn, A. Fernando, Optimization of fused deposition modeling parameters for improved PLA and ABS 3D printed structures, Int. J. Lightweight Mater. Manuf. 3 (2020) 284–297, https://doi.org/10.1016/j.ijlmm.2020.03.003.
[59] F.R. Beltrán, V. Lorenzo, J. Acosta, M.U. de la Orden, J. Martínez Urreaga, Effect of simulated mechanical recycling processes on the structure and properties of poly (lactic acid), J. Environ. Manag. 216 (2018) 25–31, https://doi.org/10.1016/j.jenvman.2017.05.020.
[60] M.-H. Hsueh, C.-J. Lai, S.-H. Wang, Y.-S. Zeng, C.-H. Hsieh, C.-Y. Pan, et al., Effect of printing parameters on the thermal and mechanical properties of 3D-printed PLA and PETG, using fused deposition modeling, Polymers 13 (2021) 1758, https://doi.org/10.3390/polym13111758.
[61] M. Żenkiewicz, J. Richert, P. Rytlewski, K. Moraczewski, M. Stepczyńska, T. Karasiewicz, Characterisation of multi-extruded poly(lactic acid), Polym. Test. 28 (2009) 412–418, https://doi.org/10.1016/j.polymertesting.2009.01.012.

[62] F.A. Cruz Sanchez, H. Boudaoud, S. Hoppe, M. Camargo, Polymer recycling in an open-source additive manufacturing context: mechanical issues, Addit. Manuf. 17 (2017) 87–105, https://doi.org/10.1016/j.addma.2017.05.013.
[63] F. Cruz, S. Lanza, H. Boudaoud, S. Hoppe, M. Camargo, Polymer Recycling and Additive Manufacturing in an Open Source Context: Optimization of Processes and Methods. International Solid Freeform Fabrication Symposium, University of Texas at Austin, 2015.
[64] L.M.G. Gonçalves, T.R. Rigolin, B.M. Frenhe, S.H.P. Bettini, On the recycling of a biodegradable polymer: multiple extrusion of poly (lactic acid), Math. Res. 23 (2020), e20200274, https://doi.org/10.1590/1980-5373-MR-2020-0274.
[65] P. Zhao, C. Rao, F. Gu, N. Sharmin, J. Fu, Close-looped recycling of polylactic acid used in 3D printing: an experimental investigation and life cycle assessment, J. Clean. Prod. 197 (2018) 1046–1055, https://doi.org/10.1016/j.jclepro.2018.06.275.
[66] E.O. Cisneros-López, A.K. Pal, A.U. Rodriguez, F. Wu, M. Misra, D.F. Mielewski, et al., Recycled poly(lactic acid)–based 3D printed sustainable biocomposites: a comparative study with injection molding, Mater. Today Sustain. 7 (8) (2020), 100027, https://doi.org/10.1016/j.mtsust.2019.100027.
[67] Printerior Recycled 3D printer Filament, Print Farm, and Large Format. Printerior n.d. https://printeriordesigns.com/(accessed November 10, 2023).
[68] 3D Printing Scraps Recycling - Canada, Toronto. FilamentsCa n.d. https://filaments.ca/pages/recycling (accessed November 10, 2023).
[69] A.L. Woern, D.J. Byard, R.B. Oakley, M.J. Fiedler, S.L. Snabes, J.M. Pearce, Fused particle fabrication 3-D printing: recycled materials' optimization and mechanical properties, Materials 11 (2018) 1413, https://doi.org/10.3390/ma11081413.
[70] E.W. Fischer, H.J. Sterzel, G. Wegner, Investigation of the structure of solution grown crystals of lactide copolymers by means of chemical reactions, Kolloid-Z. uZPolymere 251 (1973) 980–990, https://doi.org/10.1007/BF01498927.
[71] R.P. Chhabra, Non-Newtonian fluids: an introduction, in: J.M. Krishnan, A. P. Deshpande, P.B.S. Kumar (Eds.), Rheology of Complex Fluids, Springer, New York, NY, 2010, pp. 3–34, https://doi.org/10.1007/978-1-4419-6494-6_1.
[72] H.F. Giles, J.R. Wagner, E.M. Mount, Scale up, in: H.F. Giles, J.R. Wagner, E. M. Mount (Eds.), Extrusion. The Definitive Processing Guide and Handbook, William Andrew Publishing, Norwich, NY, 2005, pp. 75–77, https://doi.org/10.1016/B978-081551473-2.50008-8.
[73] ASTM D638, Standard Test Method for Tensile Properties of Plastics, 2014.
[74] J.J. Laureto, J.M. Pearce, Anisotropic mechanical property variance between ASTM D638-14 type i and type iv fused filament fabricated specimens, Polym. Test. 68 (2018) 294–301, https://doi.org/10.1016/j.polymertesting.2018.04.029.
[75] Häußge G. OctoPrint.org. OctoPrintOrg n.d. https://octoprint.org/(accessed June 23, 2023)..
[76] Standard Practice for Calculation of Color Tolerances and Color Differences from Instrumentally Measured Color Coordinates n.d. https://www.astm.org/d2244-21.html (accessed January 25, 2023).
[77] M. Korey, M.L. Rencheck, H. Tekinalp, S. Wasti, P. Wang, S. Bhagia, et al., Recycling polymer composite granulate/regrind using big area additive manufacturing, Compos. B Eng. 256 (2023), 110652, https://doi.org/10.1016/j.compositesb.2023.110652.
[78] Y. Wang, J.F. Mano, Influence of melting conditions on the thermal behaviour of poly(l-lactic acid), Eur. Polym. J. 41 (2005) 2335–2342, https://doi.org/10.1016/j.eurpolymj.2005.04.030.
[79] T. Geri, Printability Funnel: Rheological and Thermo-Mechanical Studies for Big Area Additive Manufacturing Parameters Assessment, Politecnico di Milano, 2020.
[80] J.S. Barrera Cely, RePLAy. Design of an Exhibition Kit for Fairs and Temporary Stores Using Big Area Additive Manufacturing Technology and Circular Economy Design Principles, Politecnico di Milano, 2022.
[81] Velaskello - SuperForma, SuperForma (2020). https://superforma.xyz/velaskello/. (Accessed 31 October 2022).